Hydrogeological and geophysical properties of the very slow-moving Ripley Landslide, Thompson River valley, British Columbia

David Huntley[1*], Jessica Holmes[2, 3], Peter Bobrowsky[4], Jonathan Chambers[3], Philip Meldrum[3], Paul Wilkinson[3], Shane Donohue[5], David Elwood[6], Kelvin Sattler[6], Michael Hendry[7], Renato Macciotta[7], and Nicholas Roberts[8]

1. Geological Survey of Canada, Vancouver, Canada

   * Corresponding author email: david.huntley@canada.ca

   ** Corresponding author phone: 604-365-6678

2. Queen's University Belfast, Belfast, Northern Ireland
3. British Geological Survey, Nottingham, United Kingdom
4. Geological Survey of Canada, Sidney, Canada
5. University College Dublin, Ireland
6. University of Saskatchewan, Saskatoon, Saskatchewan
7. University of Alberta, Edmonton, Alberta
8. Mineral Resources Tasmania, Department of State Growth, Rosny Park, Australia

Abstract

Landslides along a 10-km reach of Thompson River south of Ashcroft, British Columbia have repeatedly damaged vital railway infrastructure and threaten salmon runs, potable water supplies, cultural heritage features, and public safety. Government agencies, universities and the railway industry are focusing research efforts on a single test site – the very slow-moving Ripley Landslide – to better manage geohazard risk in this corridor. We characterize the landslide's composition through hydrogeological and geophysical mapping. Field mapping and exploratory drilling distinguished ten hydrogeological units in surficial deposits and fractured bedrock. Electrical resistivity tomography, frequency domain electromagnetic conductivity measurements, ground penetrating radar, seismic primary wave refraction and multispectral analysis of shear waves; in conjunction with down-hole measurement of natural gamma radiation, induction conductivity and magnetic susceptibility provide a detailed, static picture of soil moisture and groundwater conditions within the hydrogeological units. Differences in electrical resistivity of the units reflect a combination of hydrogeological characteristics, temperature and solutes. Resistive earth materials include dry glaciofluvial outwash and non-fractured bedrock; whereas glaciolacustrine clay and silt, water-bearing fractured bedrock, and saturated to partly saturated till and outwash are conductive. These new hydrogeological and geophysical datasets enhance understanding of the composition and internal structure of this landslide and provide important context to interpret multi-year monitoring underway in the valley. Continuous real-time monitoring of electrical resistivity, now underway, will help characterize water-flow paths and possible relationships to independently monitor pore pressures and slope creep.

Keywords

Surficial mapping; geophysical surveys; landslide; geohazard monitoring; British Columbia

Introduction

The ten-kilometre stretch of Thompson River between Ashcroft and Basque Ranch, British Columbia (BC) has experienced numerous landslides since the mid-1800s (**Fig. 1**). In light of threats to trans-continental transportation, Stanton (1898) investigated the earliest of these events in one of the first landslide studies in the Canadian Cordillera. Subsequent rapid failures occurred during the twentieth century (Porter et al. 2002; Clague and Evans 2003) and numerous landslides along this reach continue to creep (Eshraghian et al. 2008; Journault et al. 2018). Such instabilities have the potential to impact both of Canada's national railways, portions of Trans-Canada Highway, arable land, fisheries, and the community of Ashcroft (**Fig. 1** a). They also provide insight into landslide risk of several communities similarly situated along the inner gorge of Thompson River such as Spences Bridge, and as far south as Lytton at the confluence with Fraser River, where repeated failures have generated displacement waves or landslide dams (Drysdale 1914; Porter et al. 2002; Clague and Evans 2003).

Since 2013, Ripley Landslide has been used as a research test site to advance understanding of the composition, behaviour, and associated risks of similar but generally larger landslides along this stretch of Thompson River. The landslide occurs in unconsolidated valley fill on the east bank of the river, seven kilometres south of Ashcroft (**Fig. 1** b), and due to the small size (~3.3 ha) and continuous activity, it is an ideal target for geohazard characterization and monitoring (**Fig. 1** c, d; Bobrowsky et al. 2014, 2017). Completed and ongoing investigations at this site focus on monitoring of landslide motion and environmental conditions, through a combination of slope instrumentation, real-time global navigation satellite system (GNSS) tracking, repeat unmanned aerial vehicle (UAV) surveys, and spaceborne RADAR interferometry (InSAR) (Bunce and Chadwick 2012; Macciotta et al. 2014; Hendry et al. 2015; Journault et al. 2018). The resulting insights are guiding future landslide monitoring and geohazard mitigation efforts

in the inner gorge of Thompson River and along similar reaches of Fraser River downstream (Bobrowsky et al. 2018).

To investigate the composition of the landslide, we undertook a field-focused program combining hydrogeological mapping, stratigraphic analysis of borehole logs, geophysical testing (Huntley and Bobrowsky 2014; Huntley et al. 2017a), along with laboratory characterization of sediments and their electrical properties. Based on this work, we here characterize hydrogeological, geophysical variability and electrical properties of Ripley Landslide. These details provide important context for interpreting instrumental and remotely sensed records from the Ripley test site; and for understanding causal mechanisms and function of this and similar landslides along Thompson River.

Background: Landslides of the Thompson River Valley

Physiology, geology and climate

Thompson River occupies a broad, approximately 1 km-deep, locally steep, bedrock valley. Basement rock near Ashcroft comprises various units of the late Paleozoic to early Mesozoic Cache Creek Terrane and the largely Mesozoic Quesnel Terrane that are respectively of oceanic and island arc affinity (Monger and McMillan 1989; Gordey et al. 1991; Beatty et al. 2006). The youngest rocks, predominantly clastic sedimentary rock of the Jurassic Ashcroft Formation, are sporadically exposed along Thompson River for 10 km south of Ashcroft (Monger and McMillan 1989; Beatty et al. 2006). Above ~500 m elevation, slopes are locally mantled by colluvium or drift. Valley-bottom benchlands, reaching up to 350 m elevation, have been incised by Thompson River since the last glaciation, forming an inner gorge with steep slopes up to 125 m high.

Thick (50 m to 150 m) Pleistocene valley-bottom fill is well exposed along post-glacial terrace scarps of Thompson River and its tributaries (Ryder 1976; Clague and Evans 2003; Johnsen and Brennand 2004). These sediments include multiple glaciolacustrine units, separated by till and outwash gravel recording at least three glaciations: the last (Late Wisconsinan) glaciation, the penultimate glaciation (Early Wisconsinan), and an earlier glaciation (Ryder et al. 1991; Clague and Evans 2003). The upper part of the sediment sequence was deposited during deglaciation, when repeated glacial lake stages occupied the valley (Fulton 1969; Ryder 1976; Johnsen and Brennand 2004), and shortly after deglaciation when the valley bottom was choked by paraglacial sedimentation (Church and Ryder 1972).

Modern climate and river discharge, measured respectively 65 km east of Ashcroft at Kamloops and 40 km down Thompson River from Ashcroft near Spences Bridge, reflect seasonally variable weather conditions and hydrology. Precipitation (~250 mm, annual average) is concentrated in May to September (20 mm to 40 mm, monthly) when it falls as rain, and in December and January (20 mm to 30 mm, monthly) when it falls mainly as snow. The driest months are February to April (http://climate.weather.gc.ca/ [2018 URL]). The valley bottom is within the drought-prone Very Dry Hot subzone of the Bunchgrass biogeoclimatic zone (Nicholson et al. 1991; www.for.gov.bc.ca [2018 URL]). Thompson River discharge reflects spring snow melt and rainfall variation. Base flow varies annually from <200 m^3/s to ~600 m^3/s, with a freshet peak in late May or June of <2,000 m^3/s to >4,000 m^3/s (http://wateroffice.ec.gc.ca [2018 URL]). The river changes in elevation at Ripley Landslide by over 5 m (264.5 m to 269.8 m elevation) in response to spring melt in the surrounding mountains (Schafer et al. 2015). River levels are at their minimum between early January and early March; and start to rise in late April to early May, continuing through until late July. By early August, river levels are starting to fall.

Landslides and their drivers: initial conditions

The presence of steep slopes in bedrock and overlying fill flanking Thompson River is a necessary condition for landslide activity. During deglaciation and early post-glacial (i.e., paraglacial) time, rapid trunk valley incision in the Interior Plateau, resulting from glacio-eustatic rebound and first time exposure of poorly consolidated sediments, formed over-steepened slopes. Large, retrogressive rotational and translational landslides occurred during the Holocene (Ryder, 1976; Clague and Evans 2003). Although Pleistocene valley fill was preconditioned for failure by rapid incision of unconsolidated glacial units, landslides were most likely triggered by elevated porewater pressure during particularly wet intervals in prehistoric times. Post-glacial climate of the southern Interior Plateau has fluctuated between warmer and cooler than present conditions, but was always generally dry (Hebda 1982; Mathewes and King 1989; Hebda 1995). Even at its wettest, between 6000 and 4000 years ago, climate was not much moister than today (Hebda 1995). Thus, unconsolidated valley-bottom sediments were likely relatively dry through much of the Holocene and remained marginally stable until the 1860s when irrigation, necessary for agriculture on benchlands above the river, began (Stanton 1898; Clague and Evans 2003).

Historic failure of Pleistocene units involve one of three mechanisms (Porter et al. 2002; Clague and Evans 2003; Eshraghian et al. 2007, 2008): 1) very slow (2 cm/yr to 10 cm/yr) rotational sliding of large, intact blocks; 2) very slow (2 cm/yr to 10 cm/yr) translational sliding of blocks with little rotation; or 3) rapid flow slides and slumps, where fills disaggregate while moving down slope (>2 m/hr). Additionally, extremely rapid (>5 m/s) and very rapid (> 3 m/min) rock falls and debris falls initiate on steep valley walls (cf. Cruden and Varnes 1996), particularly in the Black Canyon. Although many landslides failed rapidly in the past, those that are

currently active are very slow-moving, reactivated compound features (Porter et al. 2002; Clague and Evans 2003; Eshraghian et al. 2007, 2008).

Possible anthropogenic triggers for historical landslides (**Fig. 1** b) include: 1) irrigation of terraces, first by leaky unlined ditches beginning in 1868, and then by confined pipes since the 1960s; and 2) excavation of lower slopes during the construction and expansion of rail lines beginning in the 1880s and continuing into this century (Stanton 1898; Clague and Evans 2003; Bunce and Chadwick 2012). Artesian groundwater pressures linked to precipitation further contribute to instability (Porter et al. 2002). Stratigraphy exerts a first order control on the distribution, geometry and rate of landslides along the inner gorge. Most failures occur along weak, sub-horizontal shear zones within glaciolacustrine clay and silt units, confined between overlying till and underlying gravel deposits and bedrock (Porter et al. 2002; Eshraghian et al. 2007, 2008; Bishop et al. 2008). Thin, highly plastic clay beds dominate the geomechanical behaviour of the glaciolacustrine units due to their low strength (Porter et al. 2002). The weakest clay zones have residual shear strengths, and were probably previously sheared during glacial overriding and syndepositional landslide events (Porter et al. 2002; Bishop et al. 2008).

Thompson River influences landslide activity in the inner gorge in several ways. Deep post-glacial incision was first required to expose weak, failure-prone units at the base of the fill sequence and provide kinematic freedom for failure (Porter et al. 2002; Clague and Evans 2003; Eshraghian et al. 2007; Bishop et al. 2008). Ongoing channel migration promotes toe instability (Porter et al. 2002) and alters landslide toe geometry (Eshraghian et al. 2008). Dropping river level exerts a complex control on landslide stability, reflecting increased hydraulic gradients within the basal glaciolacustrine unit, particularly along rupture surfaces within it (Eshraghian et al. 2008), and loss of toe loading (Porter et al. 2002; Eshraghian et al. 2008; Hendry et al.

2015). Probably because of several of these effects on toe stabilization, creep commonly accelerates shortly after flood events and during river stage drop following the freshet (Porter et al. 2002; Macciotta et al. 2014; Schafer et al. 2015).

Ripley Landslide Test Site

Ripley Landslide is approximately 220 m wide (N-S) by 150 m long (E-W) with an estimated volume of 400,000 m^3 (**Fig. 1** c). The landslide has been active since at least 1951, but displacement across the slide body increased after 2005 when a rail siding was constructed across its middle portion (Bunce and Chadwick 2012). During construction, embankments were extended upslope and a lock-block retaining wall, separating the Canadian National Railway (CN) and Canadian Pacific Railway (CP) tracks, was installed (**Fig. 1** d). Pronounced sagging of the retaining wall and bulging of lock blocks has occurred since 2005 (Huntley et al. 2016). To accommodate continual lateral and vertical displacement across the landslide, both rail companies periodically add ballast, in addition to lifting and re-aligning their tracks.

Landslide monitoring

Numerous conventional and experimental continuous monitoring technologies (**Fig. 1** c, d) provide insight on the activity, deformation mechanisms, and potential acceleration triggers of Ripley Landslide. Each of these techniques record increased landslide activity in winter, when river and groundwater levels are lowest (Macciotta et al. 2014; Hendry et al. 2015; Schafer et al. 2015; Journault et al. 2018). Four permanent GNSS monuments installed across the landslide in 2008 (**Fig. 1** c) record cumulative annual displacement on the order of 100 mm/yr to 200 mm/yr, which peaks from autumn to winter (Bunce and Chadwick 2012; Macciotta et al. 2014; Hendry et al. 2015). InSAR results from 2013 to 2015 indicate similar magnitudes and spatial-temporal patterns of displacement (Huntley et al. 2017b; Journault et al. 2018).

Ground movement concentrated within the centre of the sliding mass averages 39 mm/year, with fastest displacements detected upslope from the railway tracks and on the southern flank. Average and maximum line of sight displacement rates (equivalent to the downslope direction for the west-facing test site) of INSAR corner reflectors (**Fig. 1** c) and other coherent targets (e.g., buildings, large boulders) are 49 mm/year, and 77 mm/year, respectively; with greater displacement from November to March (Huntley et al. 2017b; Journault et al. 2018). Fibre Bragg grating (FBG) and Brillouin optical time domain reflectometry (BOTDR) monitoring of the retaining wall from 2013 to 2015 detected ~ 2 mm of accumulated strain in the wall, including displacement of individual blocks at its southern end (**Fig. 1** d), with peak activity occurring in the fall and winter months (Huntley et al. 2016; 2017c).

Subsurface borehole monitoring combining ShapeAccelArray (SAA) inclinometry with piezometer head levels indicate that the main slide body is failing along sub-horizontal, weak, basal shear surfaces in highly plastic clay beds (Macciotta et al. 2014; Hendry et al. 2015; Schafer et al. 2015). The central and northern parts of the slide are translating sub-horizontally (2.1^{o} to 2.5^{o}) whereas the southern portion near the lock-block retaining wall has a steeper (28^{o}) slide surface.

Knowledge gaps

Although earth material stratigraphy, textures and penetrative planar structures are important controls on sub-surface porosity, permeability and hydrology in the Thompson River valley (Evans 1984; Porter et al. 2002; Clague and Evans 2003), it remains unclear how these factors influence the style, timing and rate of slope displacement (i.e., form and function) at Ripley Landslide. Landslide monitoring reveals limited information on the subsurface range of earth materials, structures and hydrological behaviour. A suite of conventional terrain mapping,

geophysical methods, field sensors and laboratory techniques were tested in this challenging environment to address significant knowledge gaps in the nature and distribution of surficial earth materials, their stratigraphic relationships and internal structure of the landslide.

Methods and Results

Investigations at the Ripley Landslide test site have three aims: 1) characterizing material composition, particularly beneath railway infrastructure; 2) quantifying spatial and temporal characteristics of displacements; and 3) assessing the degree of infrastructure damage. The present study relates principally to the first objective, and provides important context for better addressing the second and third objectives. Landslide form and function in the Thompson River valley are strongly influenced by sub-surface porosity, permeability and hydrology, which are, in turn, influenced by the stratigraphic order of earth materials, textures and penetrative planar structures. To help determine the degree to which these controls influence the nature, extent and activity of Ripley Landslide, we combined terrain mapping, stratigraphic analysis of borehole logs, and several geophysical techniques to characterize hydrogeological variability at the test site.

Hydrogeological mapping

Surficial earth materials and landforms were mapped in ArcGIS using ortho-rectified and geo-referenced digital natural colour air photographs taken by a Phantom IV UAV during repeat photogrammetric overflights in September 2016, September 2017 and September 2018. The resulting imagery was sufficient to resolve cobble-sized boulders and anthropogenic features (<5 cm across) at a flight elevation 50 m above ground level. During desktop terrain analysis, visual interpretation of imagery relied on the recognition and separation of geological features using colours, tones, surface textures, patterns, shapes, sizes, shadows and field associations.

241 Fieldwork was undertaken periodically between 2013 and 2019 to ground-truth air photo
242 interpretations, and to describe sedimentological characteristics that could not be determined
243 by remote mapping. With over 80 field stations and 11 boreholes on and adjacent to the
244 landslide, hydrogeological units were defined on the basis of lithofacies and landform
245 associations, texture, sorting, colour, sedimentary structures, degrees of consolidation,
246 stratigraphic contact relationships, geological age, and other distinguishing characteristics
247 described on site (**Fig. 2** a-l). **Fig. 3** depicts the surface and vertical (stratigraphic) distribution
248 of hydrogeological units and landforms at Ripley Landslide and adjacent terrain; more detailed
249 unit descriptions are provided in Huntley and Bobrowsky (2014). Key hydrogeological
250 characteristics of these units are highlighted in **Tab. 1**. Drainage classes and permeabilities were
251 qualitatively determined from field assessments of porosity, unit thicknesses, earth material
252 textures, penetrative planar structures and slopes driving hydraulic gradients (**Tab. 1**).

253 Observations of textures and porosity variations in hydrogeological units

254 Pleistocene and Holocene sediments unconformably overlie fine-grained, massive crystalline
255 andesite (unit 1a, **Fig. 2** a) and fine-grained, flow-banded crystalline rhyolite (unit 1b) with low
256 or negligible intercrystalline porosity, and welded clast-supported agglomerates with a low
257 vugular porosity (**Fig. 2** b; **Tab. 1**). The oldest Pleistocene deposits (unit 2) are up to 6 m thick
258 and include intercalated centimetre-thick beds of clay, silt, sand, gravel and diamicton (**Fig. 3**)
259 with moderate intergranular porosity. This basal unit is disconformably overlain by up to 12 m
260 of silt-clay couplets (i.e., varves) with dropstones and stratified diamicton with low
261 intergranular porosities (**Fig. 2** c, d). Units 2 and 3 are glaciolacustrine in origin and were
262 deposited during the retreat phase of a penultimate glaciation and advance of the Late
263 Wisconsinan Cordilleran Ice Sheet, respectively. Glaciolacustrine units are over-consolidated,
264 deformed, eroded and overlain by unit 4, a massive, matrix-supported diamicton up to 5 m
265 thick composed of silt, clay, erratic boulders and ice-rafted blocks of locally derived bedrock,

interpreted as a (subglacial) lodgement till (**Fig. 2** e). Consolidation of unit 3 causes silt and clay particles to densely pack, resulting in an increase of effective stress, combined with a decrease in void ratio, water content, and permeability (Le Meil 2017). The permeability of glaciolacustrine units is anisotropic, with horizontal permeability (along the rhythmite beds) an order of magnitude larger than the vertical permeability (across beds). Heterogeneities caused by fissures and sand laminae intersecting the glaciolacustrine silt and clay significantly enhance the bulk permeability of units 2 and 3. Till has a low vugular porosity due to the presence of isolated weathered igneous and sedimentary clasts and sand-filled voids within the fine-grained matrix. Field observations, borehole logs and geophysical data all indicate that unit 4 till contains ice-rafted bedrock blocks. Silt-rich glaciolacustrine sediments (unit 5, **Fig. 2** f), containing centimetre-thick sand beds with moderate intergranular porosity, conformably overlies till. During summer months, salt crusts form where solute-rich groundwater seeps and evaporates from exposed sand-rich beds in units 3 and 5 along railway embankments and river cutbanks. Above unit 5 lies >5 m of massive and crudely stratified beds of open framework, clast-supported boulder and sand-rich gravel (unit 6, **Fig. 2** g). This coarse-grained glaciofluvial unit has a high intergranular porosity.

The oldest Holocene deposits, unit 7 (**Fig. 2** h), consist of interbedded stratified diamicton and open framework, clast-supported cobble-gravel incised into unit 6. This basal sequence fines upward to massive centimetre-thick sand and silt beds with moderate intergranular porosity. Bedding lies sub-parallel to surface slopes ranging from >3^{o} to <8^{o} on alluvial fans, and >8^{o} to <12^{o} on alluvial cones. Slopes >12^{o} are covered in postglacial coarse-grained colluvium with a high intergranular porosity (unit 8, **Fig. 2** i). Moderate slopes from >12^{o} to <26^{o} are covered in a veneer of stratified diamicton and clast-supported cobbles, boulders with interstitial sand and silt. Moderately steep bedrock slopes from >26^{o} to <35^{o} are covered in a veneer of clast-

supported talus blocks. Modern alluvial floodplain sediments (unit 9, **Fig. 2** j) are open framework, clast-supported boulders and sand with a high intergranular porosity, confined to elevations lower than 270 m. Surface water is quickly removed during heavy or prolonged rainfall, and boulders and sand are permanently saturated by river water at shallow depth (<2 m) on the active flood plain. Bedrock, glacial and alluvial sediments (units 1-5 and 9), excavated during track construction, are unconformably overlain by a linear deposit (<5 m thick) of open framework, clast-supported cobble and boulder ballast and a lock-block retaining wall (unit 10) with high intergranular porosity (**Fig. 2** k, l).

Penetrative structures observed in hydrogeological units

Unit 1 has moderate fracture porosity (**Tab. 1**). Fine-grained crystalline andesite (unit 1a) has two dominant sets of vertical joints, trending W and NW; overlying rhyolite and volcaniclastic rocks (unit 1b) have vertical fractures trending NW and SW. Volcaniclastic rocks dip eastward into the slope. These penetrative features are an expression of the regional folding and faulting history. Surface weathering rinds and mineral alteration are observed along exposed surfaces, including open fractures. Surface exposures and borehole logs reveal overlying glaciolacustrine units 2 and 3 have low to moderate fracture porosities with discrete zones where clay-rich beds are intensely cracked, fissured and sheared (**Fig. 3**). Sub-till silt and clay beds with contorted layering and loading structures indicate deformation during the overriding of glacial lake deposits by ice during the last glaciation (**Fig. 2** c, d, e). Cross-cutting (and younger) penetrative structures are observed at depths between 5 m and 15 m below surface, confined to unit 3. Below 270 m elevation. sub-horizontal planar surfaces dip from 5^{o} to 30^{o} W toward and underneath the river (**Fig. 3**, **Tab. 1**). These structures are interpreted as translational-rotational shear planes related to current landslide movement. Slide scarps, crescentic tension cracks on the slide body and surface relaxation (unloading) fractures along

316 railway embankments are sub-vertical, penetrate deep into the slide body (greater than 2 m
317 depth) and cross-cut multiple units (**Fig. 2** e, f). These penetrative structures impart a moderate
318 to high fracture porosity in till diamicton (unit 4), silt-rich glaciolacustrine beds (unit 5),
319 postglacial alluvium (unit 7), colluvial sediments (unit 8), and anthropogenic materials (unit
320 10). Coarse-grained glaciofluvial deposits (unit 6) and modern alluvial floodplain sediments
321 (unit 9) have no penetrative planar structures (**Tab. 1**).
322
323 *Geophysical field mapping*
324 The objective of the geophysical surveys was to measure contrasts in the physical properties of
325 unconsolidated sediments and bedrock, interpreted in the context of the known lithological units
326 on site (Huntley and Bobrowsky 2014; Huntley et al. 2017a, b). Geophysical surveys were
327 undertaken between 2013 and 2015 using a combination of terrestrial and waterborne electrical
328 resistivity tomography (ERT), frequency domain electromagnetic conductivity measurements
329 (FEM), ground penetrating radar (GPR), seismic primary wave refraction (PWR) and
330 multichannel analysis of surface waves (MASW); in conjunction with down-hole measurement
331 of natural gamma radiation (GR), induction conductivity (IC) and magnetic susceptibility (MS)
332 in boreholes located directly adjacent to the CPR tracks (**Fig. 3**; **Tab. 2**). Geophysical traverses
333 were spaced across the breadth of the landslide and Thompson River to ensure reasonable
334 diversity in coverage of the subsurface variability (**Fig. 4**). Terrestrial cross-sections extended
335 from behind the landslide head scarp to the channel bank (November 2013). River survey lines
336 trended parallel to the shoreline (November 2014), and were traversed using a metal-hulled jet
337 boat towing a non-metallic white-water raft containing the geophysical equipment. With regard
338 to geoelectrical properties, five terrestrial ERT lines used a Wenner-Schlumberger array with
339 48 electrodes spaced 5 m apart. Four waterborne ERT lines used a reverse Wenner array with
340 an electrode spacing of 10 m (Huntley et al. 2017a; Huntley et al. 2019a). Apparent resistivity

datasets were merged into a single file and interverted using the RES3DINV inversion program (geotomosoft.com 2017; Huntley et al. 2019b).

A Proactive Infrastructure Monitoring and Evaluation (PRIME) resistivity monitoring system was installed on the Ripley Landslide in November 2017 (Holmes et al. 2018). This system, which provides near-real time 4-D resistivity data, consists of two intersecting Wenner arrays (one 91 m long with 45 electrodes, the other 54 m long with 27 electrodes, all evenly spaced). The PRIME system is connected to the internet via a modem and allows for remote data acquisition. When calibrated with soil moisture measurements and laboratory testing of earth materials, continuous data collection allowed for changes in subsurface condition to be monitored over time (cf. Merritt et al. 2014; Uhlemann et al. 2017), and improves understanding of seasonal changes in the hydrogeological regime of the landslide (Huntley et al. 2019c).

Soil moisture monitoring

The importance of soil suctions (negative pore water pressure) on slope instability has long been recognized (Fredlund et al. 1976). Soil suctions increase the strength of soil and help stabilize slopes. However, transient near-surface changes in suction pressures, as a result of climatic conditions, may be sufficient to induce slope movement. In November 2017, two Decagon MPS6 soil suction meters were installed in the headscarp of Ripley Landslide to a depth of 2 m (Sattler et a. 2018); another three experimental meters were placed in November (**Fig. 4**). The potential use of resistivity as a proxy for suction has been previously suggested (Piegari and Di Maio 2013). In the coming years, the relationship between these parameters will be investigated using preliminary PRIME and soil suction sensor data from unit 3.

ERT results and hydrogeological units

An unprecedented level of insight into the internal composition and structure of the landslide has been gained from the terrestrial, waterborne and borehole geophysical surveys (**Tab. 2**). The ERT surveys provide the most complete and deepest penetrating information regarding the internal structure of the landslide (Huntley et al. 2017a, b; Huntley et al. 2019a, b). The FEM only images the upper 10 m, but results are consistent with ERT data, and add additional useful information on the near surface resistivity/conductivity distribution (Huntley et al. 2017a, b; Huntley et al. 2019a, b). Seismic surveys provide information on earth material stiffness at depth. GPR data show interesting results (Huntley et al. 2017a), but there are difficulties in interpretation due to the predominance of clay-rich sediments, and numberous diffracting centres, mostly boulders at various depths (**Tab. 2**).

The terrestrial-based ERT survey undertaken in November 2013 and waterbourne ERT survey completed in November 2014 are presented with PRIME data from November 2018 in a fence diagram showing the range of electrical properties of the landslide (**Fig. 5**). Since the surveys were completed at the same time of year, differences arising due to the influence of seasonal changes in weather conditions on the electrical properties were minimised by selecting November as the month of observation, and ensures that the electrical properties are comparable, although completed in different years. Data from the terrestrial-based ERT lines were inverted in 3D using Res3DInv (geotomosoft.com 2017), taking account of the offline variation in topography in the topographically complex area of the slide. This improved the correlation between each of the lines, reducing the mismatch in resistivity values at depth. The waterbourne survey data were inverted in 2D using Res2DInv (geotomosoft.com 2017). The lines are displayed in ParaView® alongside the PRIME ERT lines (**Fig. 5**).

Combined terrestrial and waterborne 2D ERT datasets are visualized as a pseudo-3D model of resistivity values using ParaView® software (**Fig. 6**). Competent bedrock (unit 1) has a high apparent resistivity value, >110 Ωm (**Fig. 6**). Weathered bedrock and colluviated fine-grained beds at the base of unit 2 are moderately resistive (80 Ωm to 110 Ωm). Overlying areas with low resistivity values (<80 Ωm) are correlated with the oldest Pleistocene glaciolacustrine sediments, units 2 and 3 (**Fig. 6**). Unit 4 lodgement till appears as a moderately resistive (80 Ωm to 110 Ωm) silt, clay and boulder diamicton up to 5 m thick (**Fig. 2** e). Silt-rich glaciolacustrine sediments (unit 5, **Fig. 2** f) have low resistivity values (<80 Ωm). Overlying glaciofluvial outwash (units 6 and 7, **Fig. 2** g) are moderately resistive (80 Ωm to 110 Ωm) when undersaturated (dry). Coarse, rapidly drained colluvium (unit 8) has a high apparent resistivity value >110 Ωm (**Fig. 6**). Modern alluvial floodplain sediments (unit 9, **Fig. 2** j) are saturated (wet) through much of the year and return high apparent resistivity values (**Fig. 6**). Coarse ballast (unit 10), when undersaturated (dry), has a high apparent resistivity >110 Ωm (**Fig. 6**).

The PRIME system has provided new insight into the hydrogeological structure of the slope (**Fig. 7**). The ERT models reveal a complex stratigraphy of coarse colluvial sediments (unit 8) overlying massive silt-rich diamicton (unit 4) with tension cracks over 0.5 m wide and 1 m deep, and highly fissured laminated silts and clays (unit 3) in which the landslide failure plane lies. Large decreases in surface resistivity (>50%) by through (March to May) are due to an increase in moisture content are due to snowmelt and intense, short-duration precipitation events. Temperatures are consistently above 0^{o}C by this time, and despite a negative weekly effective rainfall during this season, the additional moisture resulting from snowmelt is sufficient to increase the moisture content of the slope. This demonstrates the need for subsurface imaging in such locations where both temperature and precipitation control

groundwater hydrology, as this hydrogeological regime could not be predicted from weather data alone. In addition, the spatial variations in resistivity changes are also revealed, which again highlights the need for subsurface investigation. The propagation of the wetting front along the failure plane is clearly shown in **Fig. 7**, indicating that the headscarp acts as a major conduit for the flow of groundwater. Long-term monitoring of the slope will provide an insight into the seasonal variations in subsurface moisture, and combining this with near-real time displacement data will enable a long-term goal of developing moisture thresholds for failure to be realized.

Borehole geophysics results and hydrogeological units

Downhole natural GR levels, IC and MS surveys of boreholes BH15-01, BH15-02 and BH15-03 (**Fig. 3** and **Fig. 5**) provide further insight into the sub-surface thickness of earth materials, depth to bedrock, groundwater conditions and failure mechanisms of the landslide. East of the CPR tracks, the Mount Sopris MGX logging tool encountered 15 m to 17 m of glacial deposits overlying basal bedrock in the boreholes (**Fig. 5**). West of the CN tracks, boreholes show around 30 m of till and clay-rich glaciolacustrine sediments overlying bedrock (**Fig. 3** and **Fig. 5**). These observations corroborate the terrestrial and waterborne geophysics results indicating the main landslide body is located over a >20 m deep bedrock basin underlying the modern Thompson River.

Natural GR logs show a relatively constant response (**Fig. 3** and **Fig. 5**), interpreted to indicate the predominance of clays in the glacial deposits. Minor changes in readings throughout the borehole reflect small variations in sand, clay and silt content, and levels of Uranium, Thorium and Potassium in granitic and arkosic dropstones (units 2 and 3) and erratics (in unit 4) directly adjacent to boreholes. The IC logs show an initial progressive, but subtle rise in conductivity

values (**Fig. 3** and **Fig. 5**) corresponding to an increase in clay content with depth. High conductivity zones may indicate clay horizons in silt- and boulder-rich till (unit 4). At depth, conductivity levels fall in response to a lower clay content at depth (unit 3), decreasing porosity in stiff to hard silt-clay diamicton (unit 2), and electrically resistive andesite intersected in the bottom of boreholes (unit 1). The MS logs show a consistently low response (**Fig. 3** and **Fig. 5**) indicating a very low ferromagnetic mineral content in the surrounding glacial deposits (units 2 to 5). The slight decrease in MS apparent near the base of each borehole corresponds to the intersection of unconsolidated glacial deposits with andesite bedrock (**Tab. 2**).

Pertrophysical property relationships from sensor data

Petrophysical property relationships of the materials comprising the landslide complement and provide improved understanding and interpretation of field resistivity measurements. Field suction-resistivity relationships have been estabilished by relating the resistivity of the head scarp as revealed by the PRIME data with sensor data from the head scarp **(Fig. 8)**. The daily average suction is plotted alongside the daily average resistivity of the cells in the resistivity model corresponding with the suction sensor location and depth. The location of the suction sensor is shown in **Fig. 4**. Resitivity increases as suction increases. This relationship is expected, as both suction and resistivity are known to increase as moisture content decreases. A deviation from this trend is observed mid-January when daily resisitvity was higher than expected. This is likely due to localized freezing at the surface which results in increased resistivity. This is supported by the weather data, which shows temperatures below 0^{o}C around this time. Therefore, there is an increase in resistivity despite the fact that effective rainfall was positive during this period, which is usually associated with decreased resistivity.

Future work will build upon these relationships, and focus on laboratory investigations of the three different hydrogeological units present in Ripley Landslide (unit 3 - silt and clay; unit 4 - till diamicton; unit 8 – colluvial diamicton). The work will focus on the development of resistivity-moisture content, suction-moisture content, and resistivity-suction relationships for samples taken from each unit. Given the importance of temperature at this site, laboratory experiments will be carried out under a range of conditions, using temperatures recorded onsite as a basis for experimental design.

Discussion: Hydrogeological and Geophysical Properties of Ripley Landslide

Lying within the semi-arid Bunchgrass biogeoclimatic zone, slope stability at Ripley Landslide is strongly influenced by local geological properties, hydrological conditions and channel morphology. For much of the Holocene, infiltration of snow melt, precipitation and surface runoff was very limited: generally, winters and springs are dry, and summer heat causes rapid evaporation of precipitation (cf. Nicholson et al. 1991). Pleistocene and Holocene valley fill was destabilized after irrigation of benchlands began in the 1860s, and inner canyon toe slopes were excavated in the 1880s, 1950s and 2000s to accommodate CN and CPR tracks (Clague and Evans 2003; Bunce and Chadwick 2012). Surficial mapping, borehole logs, and geophysical surveys indicate the main landslide mass comprises a >20 m thick package of Pleistocene and Holocene sediments, unconformably overlying bedrock, that extends from under Thompson River to approximately 280 m elevation (**Fig. 5** and **Fig. 6**). Permeability, porosity and drainage of bedrock and surficial units in the landslide are strongly influenced by bed thicknesses, earth material textures, penetrative planar structures and slopes driving hydraulic gradients. These properties constrain the interpretation of geophysical results (**Tab. 2**) and modelling of landslide form and function.

Drainage characteristics of hydrogeological units

At the surface, electrically resistive andesite (unit 1a), rhyolite and volcaniclastic rocks (unit 1b) are relatively well-drained where moderately permeable shallow bedrock fractures and bedding planes allow downward percolation of water (**Tab. 1**). At depths >2 m, and elevations lower than 270 m (i.e., below river level), bedrock fractures with low permeability are poorly drained and remain saturated during high river stage (e.g., in spring and summer) or sealed.

More than 20 m of Pleistocene and Holocene sediment unconformably overlies unit 1 bedrock (**Fig. 3**). Locally fractured and bedded sediments of unit 2 are imperfectly drained. Below 270 m elevation, coarser sediments remain saturated for much of year, especially during higher river stages. Unit 3 is poorly drained in the sub-surface, with fine-grained sediments remaining undersaturated for much of year. The exception would be during prolonged rainfall, snow melt, sustained confined groundwater flow and high river stage. Unit 4 diamicton and clay-rich glaciolacustrine beds of unit 5 are imperfectly drained, with fractures allowing downward infiltration of surface water and subsurface flow of groundwater. Both units become saturated at depth during prolonged rainfall, snow melt and at high river stage (**Tab. 1**). At depth, vertical fractures and sub-horizontal planes become saturated during prolonged rainfall or snow melt.

Upslope of the landslide, highly permeable coarse-grained glaciofluvial sediments (unit 6) are rapidly drained. Percolating surface water and groundwater is quickly removed downslope, with subsurface flow during heavy or prolonged rainfall, and snow melt indicated by the ERT data (Huntley et al. 2019b). Moderately permeable unit 7 alluvial diamicton, silt and sand deposits are well drained, and during snow melt and heavy or prolonged rainfall, percolating water is readily removed downslope by subsurface seepage (**Tab. 1**). Highly permeable coarse-grained colluvial sediments (unit 8), alluvial floodplain deposits (unit 9), ballast, lock-block

514 retaining walls and metal culverts (unit 10) are rapidly drained, with percolating surface water
515 and groundwater quickly removed downslope, and subsurface flow occurring during heavy or
516 prolonged rainfall and snow melt (**Tab. 1**).
517
518 *Geophysical model of hydrogeological units*
519 Pseudo-3D models capture resistivity, soil moisture and groundwater conditions in surficial
520 deposits and bedrock for the fall seasons of 2013 and 2014 (**Fig. 5** and **Fig. 6**). This
521 representation is interpretation-oriented, with the selection of resistivity thresholds at 80 Ωm
522 and 110 Ωm determined by observations of earth materials, and their hydrogeological properties
523 at surface and in logged boreholes (**Fig. 2** and **Fig. 3**). Electrically resistive earth materials
524 (>110 Ωm, red on **Fig. 6**) include undersaturated (dry) sand and gravel (unit 6), till diamicton
525 (unit 4) and competent bedrock (unit 1). Bedrock, clay, till and gravel saturated with
526 groundwater are all conductive bodies (<80 Ωm, blue on **Fig. 6**). Along the north and south
527 boundaries, a transition from bedrock to saturated clay-rich glacial sediments beneath the river
528 is recorded between 220 m and 240 m elevation by a drop in resistivity values to below 80 Ωm.
529 From 240 m to 270 m elevation, conductive earth materials (<80 Ωm) are bounded by resistive
530 zones (>110 Ωm) beneath the river and east valley slope (**Fig. 6**). This pattern is interpreted to
531 represent a north-south oriented bedrock palaeochannel fragment infilled with remobilized
532 glacial deposits (units 2 and 3). The 2D waterborne ERT dataset (Huntley et al. 2017a; Huntley
533 et al. 2019a) and pseudo-3D model (**Fig. 6**) show a significant portion of the landslide lying
534 below river level from approximately 270 m to 230 m elevation. The main slide body is
535 represented as an ovate conductive zone (<80 Ωm) containing inliers of resistive material (>110
536 Ωm) along the northern, eastern and southern flanks (**Fig. 6**). These latter features are
537 interpreted as locally derived bedrock blocks remobilized during glaciation.
538

539 Conductive zones logged in the boreholes (Huntley et al. 2017a) suggest an increase in water
540 content along tension cracks, fissures, fractures and shear planes within clay, silt- and boulder-
541 rich till (unit 4) at around 5 m depth (**Fig. 3**). Deeper fissures recorded in the borehole logs and
542 field observations are not represented in the conductivity readings, suggesting lower water
543 content at these depths. Strong reflectors in GPR profiles (Huntley et al. 2017a) may also
544 represent saturated clay, silt (units 3 and 5), coarser diamictons (units 2 and 4), and bedrock
545 (unit 1) at depths < 20 m (**Tab. 2**). Higher conductivity (i.e., low resistivity, <80 Ωm) values
546 in units 2, 3 and 4 beneath the Thompson River detected by waterborne ERT (**Tab. 2**) may be
547 attributed changes in clay and groundwater content of sub-river units. Three zones of elevated
548 terrain conductivity across the submerged landslide toe have been identified in the bathymetry-
549 corrected waterborne FEM data (**Fig. 6**), These zones are interpreted to indicate areas where
550 artesian groundwater in units 2, 3 and 4 is discharging through the boulder lag (unit 9) covering
551 the river bed (Huntley et al. 2017a; Huntley et al. 2019a).
552
553 Upslope of the river floodplain and railway ballast, at elevations from 270 m to 295 m,
554 resistivity values >110 Ωm are intersected. This range in values is consistent with unsaturated
555 silt, sand and cobble colluvium overlying bedrock (**Fig. 6**). The distribution of these units
556 suggests a 290 m elevation limit to eastward headscarp retrogression and potential maximum
557 volume of approximately 0.8 x 10^6 m^3 for the landslide. Above the head scarp, zones of higher
558 conductivity occur where soil water is migrating toward the water table through silt, sand and
559 cobbles exposed by hill slope erosion (**Fig. 6**). Upslope of the landslide, zones of high resistivity
560 (>80 Ωm) in units 5, 6 and 7 occur where soil water is migrating toward the water table through
561 silt, sand and cobbles exposed by gully erosion (**Tab. 2**; **Fig. 5**).
562
563 *Landslide function: observations of hydrogeology and geophysical data*

Fluctuations in stream discharge and river level affect the stability of Ripley Landslide in three ways: 1) by changing the porewater pressure on the rupture surfaces in units 2, 3 and 4; 2) by changing the loading pressure on the submerged toe slope; and 3) by altering the slide geometry through cutbank erosion, channel incision and toe scour. An increase in slope instability occurs during years when the river level is elevated above average for longer than normal periods. During spring run-off, high water levels provides temporary loading support at the landslide toe, resulting in slower movement rates. Higher ground movement rates occur during autumn and winter when river discharge and groundwater levels drop, reducing load values on the slide toe and porewater pressures in the main body (cf. Eshraghian et al. 2007; Hendry et al. 2015; Journault et al. 2018).

Elsewhere in the Thompson River valley, failing glaciolacustrine beds are highly plastic, with plastic/liquid limits ranging from 45% to 90% and residual friction angles of 10^{o} to 15^{o} (Schafer et sl. 2015; Le Meil 2017). Silt beds in units 2, 3 and 5 have higher overall residual shear strength compared to clay beds, with values ranging from $>26^{o}$ to $<35^{o}$ (cf. glacial pond to steep-dipping silt-rich debris flow diamictons draped over bedrock in **Fig. 2** c). At Ripley Landslide, field observations and borehole logs show that deformation and erosion by glaciers or pre-historic slope movement have created pre-sheared discontinuities in units 2, 3 and 4 (**Fig. 2** d) at a residual strength that predispose these sediments to failure (cf. Clague and Evans 2003; Eshraghian et al. 2007; 2008). Fine-grained glacial sediments (units 2 to 4) have low permeability (**Tab. 1**) and exhibit subtle resistivity changes reflecting variations in total clay and groundwater content across the slide body (**Fig. 6**).

Seasonal wetting and softening of clay beds may contribute to slope failure (cf. Clague and Evans 2003). Surface and borehole monitoring indicate that much of the landslide moves very

589 slowly (cumulatively <55 mm/yr) on gentle (<2°) channel-sloping failure planes developed in
590 weak, highly plastic layers of fine-grained glaciolacustrine silt and clay (**Fig. 3**). Failure of units
591 2 to 5 occurs as shear strength is reduced in response to periods of saturation when the residual
592 friction angle of clay layers falls below the angle of slope (generally <25°). The ERT data show
593 that these failing sediments are conductive (<80 Ωm), potentially saturated with groundwater,
594 and extend under the river (**Fig. 6**). Sediments of units 2 to 5 readily move, even on gentle
595 slopes, due to a reduction in shear strength with increasing saturation of sediments and
596 penetrative structures. All other surficial units contain little clay, are non-plastic and permeable
597 to some degree. The presence of penetrative structures (e.g., tension cracks and slide surfaces),
598 bedding thickness and porewater pressure in sand and gravel beds within glaciolacustrine units
599 influence the effective stress condition of the slope (cf. Clague and Evans 2003; Bishop et al.
600 2008). The residual friction angle of clay beds in glaciolacustrine units is stress dependant: high
601 normal stresses promote alignment of clay particles during shear (Schafer et al. 2015; Le Meil
602 2017). Greater normal stresses beneath the main body of the landslide are expected where
603 InSAR and GNSS measurements show rates of movement are highest, and where geophysical
604 data indicate surficial deposits are >20 m thick. While the rate of movement is very slow, rapid
605 failure is possible under certain conditions. For example, when surface tension cracks fill with
606 infiltrating water (or snow) and landslide debris becomes saturated by rising river and
607 groundwater levels.
608
609 Waterborne geophysical surveys reveal that the landslide extends under Thompson River,
610 where sediments are generally <20 m thick and river levels vary seasonally by >2 m. Fine-
611 grained beds (units 3 and 4) in the submerged toe are armoured from erosion by a lag deposit
612 of modern fluvial boulders (unit 9) except where a deep trough and scour pool is carved by
613 strong currents (**Fig. 4**). Here, bedding and sliding surfaces are exposed at the bottom or slightly

614 below the riverbed (<270 m elevation). For the submerged toe, shear rates are likely to be lower,
615 variable and stage-dependent (cf. Porter et al. 2002; Schafer et al. 2016). Scour holes and
616 cutbank erosion are evidence that the river continues to incise the channel floor (**Fig. 4**) when
617 rock fall debris (unit 8) constricts stream flow, locally increasing current velocity. Higher rates
618 of landslide movement might be triggered along deep-seated rupture planes if plastic clay beds
619 near the top of unit 3 (seen in borehole logs, e.g., **Fig. 6**) become exposed during channel
620 incision. Cutbank erosion is also producing over-steepened toe blocks along the main channel.
621 If these blocks fail and are removed when river and groundwater levels are low, toe slope
622 unloading may contribute to rapid movement on rupture surfaces (cf. Eshraghian et al. 2007).
623 Toe slope incision is occurring adjacent to where the highest ground motion rates are recorded
624 on the landslide (Macciotta et al. 2015; Hendry et al. 2015; Journault et al. 2018). This is also
625 where critical railway infrastructure is at risk (i.e., the lock-block retaining wall and tracks; **Fig.**
626 **1** d). The seasonal addition of ballast, combined with longer, heavier and more frequent trains
627 crossing the main slide body may also contribute to subaerial loading. It is not known whether
628 these factors trigger increased movement during times of reduced shear strength.
629
630 Lastly, extreme weather events and climate change have the potential to exacerbate ongoing
631 landslide activity at the test site. Although the average rainfall in the area has increased since
632 the 1920s, there is no direct correlation with landslide activity (Porter et al. 2002; Eshraghian
633 et al. 2007). However, increased duration and magnitude of precipitation, loss of vegetation
634 cover, reduced soil cohesion by wildfires and fluctuating river discharge could contribute to
635 sustained periods of groundwater recharge, increased porewater pressures in bedrock and
636 surficial units, higher seasonal river discharges and greater channel erosion triggering additional
637 landslide activity in the Thompson River valley. Irrigation water does not directly contribute to
638 instability of Ripley Landslide since the surrounding slopes are still used as rangeland.

However, grazing limits the already sparse vegetation cover and cattle trails form intermittent linear paths of disturbed soil forming narrow slope breaks that contour slopes. These conditions contribute to infiltration of precipitation, snow melt and surface runoff into the unconsolidated valley fill.

Summary and Conclusions

The overarching goal of our work is the mitigation of risks to public safety, the environment, and railway transportation infrastructure. Studies of Ripley Landslide provide important insight into processes and behaviour of similar, but much larger, landslides between Ashcroft and Basque Ranch (**Fig. 1**). Like others landslides in the Thompson River valley (Porter et al. 2002; Clague and Evans 2003; Eshraghian et al. 2007), seasonal movement occurs along sub-horizontal translational rupture surfaces corresponding to weak glacially sheared zones in glaciolacustrine clay and silt (unit 3) and till (unit 4) (**Fig. 3** and **Fig. 5**). This constant activity has the potential to cause damage to railway tracks and disruption of service with risks to the national economy, the local environment, and natural resources (e.g., potable water and salmon).

Significant gaps in the knowledge of the nature of bedrock and surficial earth materials, their stratigraphic relationships; and in the controls on the style of mass wasting have been addressed here. By combining terrain analysis and modelling of multidimensional geophysical datasets, we have revealed an unprecedented level of detail in the internal composition, structure and hydrology of the very slow-moving Ripley Landslide. This paper helps to explain how hydrogeological conditions influence the spatial and temporal patterns of surface water and groundwater flow; and how future changes in climate and landscape conditions might influence landslide activity along Thompson River.

664

665 At the test site, >20 m of glacial deposits with contrasting porosity and permeability are
666 preserved in a fractured bedrock paleo-channel basin. Bedrock and unconsolidated sediments
667 have been subaerially exposed by post-glacial valley incision, and during construction of the
668 railway corridor since the late 19th century. The pool and riffle channel morphology of
669 Thompson River at Ripley Landslide is significant because hydraulic conductivity between the
670 river, landslides and groundwater systems likely increases where fractured bedrock and
671 glaciolacustrine units (containing impermeable silt-clay couplets, coarse porous beds, lateral
672 failure planes and vertical tension cracks) are continually exposed by fluvial erosion. Scour
673 pools are also identified adjacent to irrigated benchlands along the study reach. These terraces
674 are potentially unstable and should be monitored together with active landslides for surface
675 subsidence, tension cracks and scarps to better manage geohazard risks in the Thompson River
676 valley.

677

678 Field observations (**Tab. 1**) and geophysical data (**Tab. 2**) indicate that Pleistocene units 4 to
679 7 host an unconfined aquifer recharged by infiltrating precipitation and surface runoff across
680 Ripley Landslide, and from the slopes above. Soil water and groundwater flow laterally and
681 downward through porous till and glaciofluvial sediments (units 4 and 6), and through
682 vertically fractured glaciolacustrine units (3 and 5), until it encounters fractured, non-porous
683 bedrock (unit 1) or sub-horizontal shear zones in unit 3. As with other landslides in the area,
684 units 2, 3 and 5 function as aquitards, but also accommodate landslide movement and porewater
685 migration along shear zones approximately corresponding to stratigraphic boundaries (**Fig. 5**).
686 Artesian conditions at the landslide toe suggest the presence of an aquifer in unit 1 (bedrock)
687 and unit 2 (diamicton), confined by clay and silt layers in units 2 and 3 (cf. Macciotta et al.
688 2014; Hendry et al. 2015; Schafer et al. 2015). Recharge sources include groundwater flow

through buried paleochannels and along unconformities separating older glacial sequences (cf. Porter et al. 2002; Clague and Evans 2003). This confined aquifer controls porewater pressures at the base of unit 3.

A continuous (real-time) proactive infrastructure monitoring and evaluation (PRIME) system has now been deployed to characterize the long-term hydrological behaviour of the landslide by monitoring dynamic (pseudo-4D) changes in electrical resistivity (cf. Merritt et al. 2014; Uhlemann et al. 2017; Huntley et al. 2019b). To establish the petrophysical relationship linking resistivity to moisture content, laboratory testing of three samples (units 3, 4 and 8), collected across the landslide, was undertaken at the British Geological Survey facilities at Keyworth, UK. A continuous dataset will help to better define: 1) contributions from surface runoff, precipitation, freeze-thaw cycles, and snow melt to seasonal variations in slope movement; 2) surface water and groundwater flow paths through the main slide body, the river and bedrock; and 3) the relationship of fluctuating porewater pressures monitored in boreholes and landslide activity. Relationships between suction and resistivity derived from field data (Holmes et al. 2018; Sattler et al. 2018) demonstrate the importance of changing moisture content (and therefore changing suction and pore pressures) for resistivity, but given the wide range of geological units present on the site, understanding the hydrogeological properties of each unit will be pivotal in providing improved understanding of slope stability in the Thompson River valley. As such, future work will focus on the laboratory testing of samples from different units of the Ripley landslide, building upon relationships identified in the field to establish relationships between moisture content, suction and resistivity. These relationships will then be used to better constrain the inversion of the ERT data. This new understanding will guide the interpretation of multi-year monitoring datasets (e.g., GNSS, InSAR) and future efforts to track landslide activity in the Thompson River valley.

Acknowledgements

Research was undertaken as part of the International Consortium on Landslides (ICL) International Programme on Landslides (IPL) Project 202. Activities at this site have led to World Centre of Excellence on landslide disaster reduction recognition for both the Geological Survey of Canada and the University of Alberta (iplhq.org). Research was funded by Transport Canada and Natural Resources Canada. For their geophysical services, we wish to thank Neil Parry, Megan Caston, Cassandra Budd and Gordon Brasnett (EBA-TetraTech, Edmonton, Alberta) in 2013-2014; Paul Bauman, Landon Woods and Kimberly Hume (Advisian, Worley Parsons Group, Calgary, Alberta) in 2014-2015; Cliff Candy, Larry Theriault, Caitlin Gugins and Heather Ainsworth (Frontier Geosciences Inc., North Vancouver, BC) in 2015-2017; and Mel Best (BEMEX Consulting International, Victoria, BC). The PRIME installation (2017 to present) is a collaboration with Helen Reeves and colleagues (British Geological Survey, Nottingham, UK). Fieldwork would not be possible without the support of Trevor Evans (Canadian National Railway, Kamloops, BC) and Danny Wong and Jason Bojey (Canadian Pacific Railway, Calgary, Alberta). The contribution of Jessica Holmes was funded by the Department for the Economy (DfE), Northern Ireland.

References

Beatty, T.W., Orchard, M.J., and Mustard, P.S. 2006. Geology and tectonic history of the Quesnel terrane in the area of Kamloops, British Columbia. *In* Paleozoic evolution and metallogeny of pericratonic terranes at the ancient pacific margin of North America, Canadian and Alaskan Cordillera. Geological Association of Canada, Special Paper, **45**: 483-504

739 Bishop, N., Evans, S., Petley, D., and Unger, A. 2008. The geotechnics of glaciolacustrine
740 sediments and associated landslides near Ashcroft (British Columbia) and the Grand Coulee
741 Dam (Washington). *In* From Causes to Management. 4th Proceedings of the Canadian
742 Conference on Geohazards, 594 p
743
744 Bobrowsky P., Sladen W., Huntley, D., Zhang, Q., Bunce, C., Edwards, T., Hendry, M.,
745 Martin, D., and Choi, E. 2014. Multi-parameter monitoring of a slow moving landslide:
746 Ripley Slide, British Columbia, Canada. *In* Engineering Geology for Society and Territory -
747 Volume 2, Landslide Processes, IAEG Congress, Springer Publishing, pp. 155-159
748
749 Bobrowsky P., Huntley D., Neelands P, MacLeod R, Mariampillai D, Hendry M, Macciotta
750 R, Reeves H., and Chambers J. 2017. Ripley Landslide – Canada's premier landslide field
751 laboratory. Geological Society of America, Annual Meeting Abstracts and Proceedings
752 Volume, 1 p
753
754 Bobrowsky, P., MacLeod, R., Huntley, D., Niemann, O., Hendry, M. and Macciotta, R. 2018.
755 Ensuring Resource Transport Safety: Monitoring Critical Infrastructure with UAV
756 Technology. Resources for Future Generations, Proceedings Volume and Abstracts,
757 Vancouver, Canada, 1 p
758
759 Bunce C. and Chadwick, I. 2012. GPS monitoring of a landslide for railways. In: Eberhardt
760 E, et al (eds) Landslides and Engineered Slopes - Protecting Society through Improved
761 Understanding: 1373-1379
762

763 Church, M., Ryder, J.M. 1972. Paraglacial sedimentation: a consideration of fluvial processes
764 conditioned by glaciation. Geological Society America, Bulletin 83: 3059–3072
765
766 Clague, J. and Evans, S. 2003. Geologic framework for large historic landslides in Thompson
767 River valley, British Columbia. Environmental and Engineering Geoscience **9** (3): 201-212
768
769 Cruden, D.M. and Varnes, D.J. 1996. Landslide types and processes. *In* Landslides,
770 Investigation and Mitigation. Washington Transportation Research Board, Special Report
771 **247**: 36 -75
772
773 Deblonde, C., Cocking, R.B., Kerr, D. E., Campbell, J.E., Eagles, S., Everett, D., Huntley,
774 D.H., Inglis, E., Parent, M., Plouffe, A., Robertson, L., Smith, I.R. and Weatherston, A. 2018.
775 Surficial Data Model: the science language of the integrated Geological Survey of Canada
776 data model for surficial geology maps. Geological Survey of Canada, Open File 8236, (ed.
777 version 2.3.14), 50 p, (2 sheets)

778 Drysdale, C.W. 1914. Geology of the Thompson River valley below Kamloops Lake, B.C. *In*
779 1912 Summary Report, Geological Survey, Department of Mines Sessional Paper, **26**: 115-
780 150
781
782 Eshraghian, A., Martin, C. and Cruden, D. 2007. Complex earth slides in the Thompson
783 River Valley, Ashcroft, British Columbia. Environmental and Engineering Geoscience XIII:
784 161-181
785

786 Eshraghian, A., Martin, C. and Morgenstern, N. 2008. Movement triggers and mechanisms of
787 two earth slides in the Thompson River Valley, British Columbia, Canada. Canadian
788 Geotechnical Journal, **45**: 1189-1209
789
790 Evans, S.G. 1984. The 1880 landslide dam on Thompson River, near Ashcroft, British
791 Columbia. In: Current Research, Part A: Geological Survey of Canada Paper 84-1A: 655–658
792
793 Fredlund, D.G., Morgenstern, N.R. and Widger, R.A. 1976. The shear strength of unsaturated
794 soils. Canadian Geotechnical Journal, **13**: 261-275
795
796 Fulton, R.J. 1969. Glacial Lake History, Southern Interior Plateau, British Columbia.
797 Geological Survey of Canada, Paper 69-37, 14 p
798
799 Gordey, S.P., Geldzetzer, H.H.J., Morrow, D.W., Bamberm, E.W., Henderson, C.M.,
800 Richards, B.C., McGugan, A., Gibson, D.W. and Poulton, T.P. 1991. Ancestral North
801 America, Part A. *In* Upper Devonian to Middle Jurassic assemblages, Chapter 8 of Geology
802 of the Cordilleran Orogen in Canada, Geology of Canada, Geological Survey of Canada, **4**:
803 219-327
804
805 Hebda, R.J. 1982. Postglacial history of grasslands of southern British Columbia and adjacent
806 regions. *In* Grassland Ecology and Classification Symposium Proceedings. British Columbia
807 Ministry of Forests, pp. 157-191
808
809 Hebda, R.J. 1995. British Columbia vegetation and climate history with focus on 6 ka B.P.
810 Geographic Physique et Quaternaire, **49**: 55-79

Hendry, M., Macciotta, R. and Martin, D. 2015. Effect of Thompson River elevation on velocity and instability of Ripley Slide. Canadian Geotechnical Journal, **52** (3): 257-267

Huntley, D. and Bobrowsky, P. 2014.Surficial geology and monitoring of the Ripley Slide, near Ashcroft, British Columbia, Canada. Geological Survey of Canada, Open File 7531, 21 p

Huntley, D., Bobrowsky, P., Zhang, Q., Zhang, X., Lv, Z., Hendry, M., Macciotta, R., Schafer, M., Le Meil, G., Journault, J. and Tappenden, K. 2016. Application of Optical Fibre Sensing Real-Time Monitoring Technology at the Ripley Landslide, near Ashcroft, British Columbia, Canada. Canadian Geotechnical Society, GeoVancouver 2016 Annual Meeting Proceedings Volume, 13 p

Huntley, D., Bobrowsky, P., Parry, N., Bauman, P., Candy C. and Best, M. 2017a. Ripley Landslide: the geophysical structure of a slow-moving landslide near Ashcroft, British Columbia, Canada. Geological Survey of Canada, Open File 8062, 59 p

Huntley, D., Bobrowsky, P. and Best, M. 2017b. Combining terrestrial and waterborne geophysical surveys to investigate the internal composition and structure of a very slow-moving landslide near Ashcroft, British Columbia, Canada. *In* Landslide Research and Risk Reduction for Advancing Culture and Living with Natural Hazards - Volume 2, 4th World Landslide Forum (ICL-IPL), Springer Nature, 15 p

Huntley, D., Bobrowsky, P., Zhang, Q,, Zhang, X, and Lv, Z. 2017c. Fibre Bragg Grating and Brillouin Optical Time Domain Reflectometry Monitoring Manual for the Ripley Landslide, near Ashcroft, British Columbia. Geological Survey of Canada, Open File 8258, 66 p

Huntley, D., Bobrowsky, P., Hendry, M., Macciotta, R. and Best, M. 2019a. Multi-technique geophysical investigation of a very slow-moving landslide near Ashcroft, British Columbia, Canada. Journal of Environmental and Engineering Geophysics, **24** (1): 85-108

Huntley, D., Bobrowsky, P., Hendry, M., Macciotta, R., Elwood, D., Sattler, K., Best, M., Holmes, J., Chambers, J., Meldrum, P. and Wilkinson, P. 2019b. Application of multi-dimensional electrical resistivity tomography datasets to investigate a very slow-moving landslide near Ashcroft, British Columbia, Canada. Landslides, **16** (5):1033-1042

Huntley, D., Bobrowsky, MacLeod R., Cocking, R., Joseph, J., P., Slatter, C., Elwood, D., Holmes, J., Chambers, J., Meldrum, P., Wilkinson, Hendry, M., and Macciotta, R. 2019c. PRIME installation in Canada: protecting national railway infrastructure by monitoring moisture in an active slow-moving landslide near Ashcroft, British Columbia. Geological Survey of Canada, Open File 8548, 1 poster

Journault, J., Macciotta, R., Hendry, M., Charbonneau, F., Huntley, D. and Bobrowsky, P. 2018. Measuring displacements of the Thompson River valley landslides, south of Ashcroft, B.C., Canada, using satellite InSAR. Landslides **15** (4): 621-636.

Le Meil, G. 2017. Characterization of a landslide-prone glaciolacustrine clay from the Thompson River Valley near Ashcroft, British Columbia. Department of Civil and

Environmental Engineering, University of Alberta, Masters of Science in Geological Engineering, 182 p

Macciotta, R., Hendry, M., Martin, D., Elwood, D,, Lan, H., Huntley, D., Bobrowsky, P., Sladen, W., Bunce, C., Choi, E. and Edwards, T. 2014. Monitoring of the Ripley Slide in the Thompson River Valley, B.C. Geohazards 6 Symposium, Proceedings and Abstracts Volume, Kingston, Ontario, Canada, 1 p

Mathewes, R.W. and King, M. 1989. Holocene vegetation, climate, and lake-level changes in the Interior Douglas-Fir biogeoclimatic zone, British Columbia. Canadian Journal of Earth Sciences, **26**: 1811-1825

Merritt, A., Chambers, J., Murphy, W., Wilkinson, P., West, L., Gunn, D., Meldrum, P., Kirkham, M. and Dixon, N. 2014. 3D ground model development for an active landslide in Lias mudrocks using geophysical, remote sensing and geotechnical methods. Landslides, **11** (4): 537-550

Monger, J.W.H. and McMillan, W.J. 1989. Geology, Ashcroft, British Columbia (92 I). Geological Survey of Canada, Map 42-1989, Scale 1:250,000

Nicholson, A., Hamilton, E., Harper, W.L., Wikeen, B.M. Bunchgrass Zone – Chapter 8. In: Meidinger, D. and Pojar, J. 1991. Ecosystems of British Columbia. B.C. Ministry of Forests, Special Report 6: 125-137

884 Piegari, E. and Di Maio, R. 2013. Estimating soil suction from resistivity. Natural Hazards
885 Earth Systems Science, **13**: 2369-2379
886
887 Porter, M., Savigny, K., Keegan, T., Bunce, C. and MacKay, C. 2002. Controls on stability of
888 the Thompson River landslides. In: Proceedings of the 55th Canadian Geotechnical
889 Conference: Ground and Water – Theory to Practice, Canadian Geotechnical Society, pp.
890 1393-1400
891
892 RES3DINV (2017 [URL]) Rapid 3-D Resistivity & IP inversion using the least-squares
893 method, Geoelectrical Imaging 2D & 3D Geotomo Software Version 3.14, Available from
894 www.geotomosoft.com [accessed April, 2019]
895
896 Ryder, J.M. 1976. Terrain inventory and Quaternary geology, Ashcroft, British Columbia.
897 Geological Survey of Canada, Paper 74-79, 17 p
898
899 Ryder, J.M., Fulton, R.J. and Clague, J.J. 1991. The Cordilleran Ice Sheet and the Glacial
900 Geomorphology of Southern and Central British Colombia. Géographie physique et
901 Quaternaire, **45** (3): 365–377
902
903 Schafer, M., Macciotta, R., Hendry, M., Martin, D., Bobrowsky, P., Huntley, D., Bunce, C.
904 and Edwards, T. 2015. Instrumenting and Monitoring a Slow Moving Landslide. GeoQuebec
905 2015 – Challenges from North to South, 7 p
906
907 Stanton, R.B. 1898. The great land-slides on the Canadian Pacific Railway in British
908 Columbia. Proceedings of Civil Engineers **132** (2): 1–48

Uhlemann, S., Chambers, J., Wilkinson, P., Maurer, H., Merritt, A., Meldrum, P., Kuras, O., Gunn, D. and Dijkstra, T. 2017. Four-dimensional imaging of moisture dynamics during landslide reactivation. Journal of Geophysical Research (Earth Surface), **122**: 398-418

Tables

Table 1 Hydrogeological characteristics of Ripley Landslide.

Hydro-geological Unit (thickness, m)	**Earth material textures (and Porosity)** Intercrystalline porosity Intergranular porosity Vugular porosity **H** (high porosity), **M** (moderate porosity) or **L** (low porosity)	**Penetrative structures (and Porosity)** Fracture porosity **H** (high porosity), **M** (moderate porosity) or **L** (low porosity)	**Drainage (and Permeability)** Rate at which surface water and groundwater flows through unit: **H** (high permeability), **M** (moderately permeability) or **L** (low permeability)
Unit 10 Anthro-pogenic materials (<2 m – 5 m)	Intergranular porosity (**H**) Open framework, clast-supported cobble and boulder ballast	Fracture porosity (**H**) • Displacement of concrete lock-blocks • Sub-vertical crescentic tension cracks in ballast	Rapidly drained (**H**) Percolating surface water quickly removed downslope during heavy or prolonged rainfall
Unit 9 Alluvial sediments (<2 m)	Intergranular porosity (**H**) Open framework, clast-supported boulders and sand		Rapidly drained (**H**) Percolating surface water quickly removed downslope during heavy or prolonged rainfall; permanently saturated at shallow depth (<2 m)
Unit 8 Hillslope colluvial sediments (<2 m)	Intergranular porosity (**H**) Talus blocks veneer steep bedrock slopes Stratified diamicton and clast-supported cobbles, boulders with interstitial sand and silt veneer unconsolidated slopes	Fracture porosity (**H**) • Sub-vertical crescentic tension cracks oriented N-S on slide body	Rapidly drained (**H**) Percolating surface water and groundwater quickly removed downslope, with subsurface flow during heavy or prolonged rainfall
Unit 7 Alluvial fan sediments (<2 m)	Intergranular porosity (**M**) Basal interbedded stratified diamicton and open framework, clast-supported cobble-gravel, fining upward to massive sand and silt; cm-thick beds sub-parallel to surface slopes from 3º to 8º (fans) and >8º to <12º (cones)	Fracture porosity (**H**) • Sub-vertical crescentic tension cracks oriented N-S on slide body	Well drained (**M**) Percolating surface water readily removed downslope, with subsurface seepage during heavy or prolonged rainfall
Unit 6 Glaciofluvial sediments (2 m to >5 m)	Intergranular porosity (**H**) Massive and crudely stratified, open framework, clast-supported boulder and sand-rich gravel beds, m-thick beds		Rapidly drained (**H**) Percolating surface water and groundwater readily removed downslope, with subsurface flow during heavy or prolonged rainfall
Unit 5 Glacio-lacustrine sediments (<2 m to 5 m)	Intergranular porosity (**M**) Pebble-rich sand; cm-thick interbeds	Fracture porosity (**M**) Rhythmically interbedded silt, clay and diamicton, cm-thick with: • Sub-vertical N-S unloading fractures parallel to exposed slope • Sub-vertical crescentic tension cracks oriented N-S on slide body • Fissile partings parallel to bedding, dipping W into bedrock basin	Imperfectly drained (**L**) Seepage from exposed porous sand-rich interbeds indicated by salt crusts form at surface during summer months along the railway and river embankments; at depth, fractures become saturated during prolonged rainfall
Unit 4 Glacial till sediments (2 m to 6 m)	Vugular porosity (**L**) Massive, matrix-supported diamicton composed of silt, clay and boulders, isolated weathered clasts and sand-filled voids; m-thick beds	Fracture porosity (**M**) • Sub-vertical unloading fractures sub-parallel to exposed slopes, oriented N-S • Sub-vertical crescentic tension cracks oriented N-S on slide body • Sub-horizontal shear surfaces below 270 m elevation, dipping W into bedrock basin	Imperfectly drained (**L**) Fractures allow downward and subsurface flow of groundwater; fractures become saturated at depth during prolonged rainfall and during high river stage
Unit 3 Glacio-lacustrine sediments (5 m to >15 m)	Intergranular porosity (**M**) Sand and gravel; cm-thick interbeds; uncommon	Fracture porosity (**L**) Rhythmically interbedded clay and silt and diamicton, mm-thick with: • Sub-vertical N-S oriented unloading fractures parallel to exposed slope • Sub-vertical crescentic tension cracks oriented N-S on slide body	Poorly drained (**L**) Sub-surface sediments remain undersaturated for much of year, except during prolonged rainfall, sustained confined groundwater flow and during high river stage

		• Contorted bedding and loading structures • Fissile partings parallel to bedding, dipping W into bedrock basin • Sub-horizontal shear surfaces below 260 m elevation, dipping W into bedrock basin	
Unit 2 Glacio-lacustrine sediments (<2 m to 6 m)	Intergranular porosity (**M**) Sand, gravel, stratified clast-supported diamicton; cm-thick interbeds	Fracture porosity (**L**) Silt, clay and matrix-supported diamicton; cm-thick; with: • Fissile partings along bedding planes dipping W into bedrock basin	Imperfectly drained (**L**) Fissile, bedded sediments remain saturated for much of year
Unit 1b Rhyolite[1] and Volcaniclastic rocks[2] (>2 m)	Vugular porosity (**L**) [2]Welded, clast-supported agglomerate Intercrystalline porosity (**L**) [1]Fine-grained, flow-banded crystalline igneous rock [1,]	Fracture porosity (**M**) • [2]Bedding planes, *<20° NNE* • [1,2]Dominant fracture sets, *NW – SW* • Weathering rinds along fracture surfaces • Fractures sealed at depth	[1,2]Well drained (**M**) Shallow bedrock fractures and bedding planes allow downward and subsurface flow of groundwater [1,2]Poorly drained (**L**) At depth, fractures saturated for much of year, or too tight for water flow
Unit 1a Andesite (>2 m)	Intercrystalline porosity (**L**) Fine-grained, massive crystalline igneous rock	Fracture porosity (**M**) • Dominant fracture sets, *E – NW* • Weathering rinds along fracture surfaces • Fractures sealed at depth	Well drained (**M**) Shallow bedrock fractures and bedding planes allow downward and subsurface flow of groundwater Poorly drained (**L**) At depth, fractures saturated for much of year, or too tight for water flow

921

922

923

Table 2 Summary of modelled terrestrial and waterborne ERT, FEM, GPR and Seismic properties of surficial units and bedrock at Ripley Landslide; * groundwater seeps / ** groundwater in fractures, partings and porous beds / *** downward percolating surface waters; GPR reflectors, P – point, L – linear, S- strong, M – moderate, W – weak.

Hydro-geological Unit	**Earth Material** Description; structure; drainage	**T-ERT** Ωm	**W-ERT** Ωm	**T-FEM** Modelled conduct-ivity mS m^{-1} *Resistivity Ωm*	**W-EM** Modelled conduct-ivity mS m^{-1} Bathymetry corrected *Resistivity Ωm*	**T-GPR, W-GPR** Origin, character, strength of reflectors	**Seismic Refraction** P-wave velocity m s^{-1}	**Shear Wave** Velocity m s^{-1}
Unit 10 */*** Anthro-pogenic	Cobble and boulder ballast; rapidly-drained	<500	-	<5 *>200*	-	Boulders P, S Unit contact L, W	250 - 600	240 - 280
Unit 9 */* Alluvial *May contain ground-water seeps*	Boulders and sand; rapidly drained; saturated	<500	100 - 450	<5 *>200*	30 – 60 *33 - 17*	Boulders P, S Unit contact L, W	600 - 3500	240 - 280
Unit 8 */* **C**olluvial	Blocks, gravel, sand, clast-supported diamicton; rapidly-drained	<500	-	<20 *>50*	-	Boulders P, M - S Unit contact L, W	250 - 600	100 - 240
Unit 7 */* Alluvial	Sand, silt and minor gravel; well-drained	125 - 500	-	<20 *>50*	-	Basal contact L, W	250 - 600	100 - 200
Unit 6 *** Glaciofluvial	Gravel and sand; rapidly-drained	125 - 500	-	<20 *>50*	-	Boulders P, M Basal contact L, W	250	100 - 280
Unit 5 */** Glacio-lacustrine	Silt and clay; deformed; imperfectly-drained	<125	-	>20 *<50*	-	Groundwater L, W - M Basal contact L, W - M	1400 – 2300	240 - 300
Unit 4 **/*** Till	Silt-clay matrix-supported diamicton; imperfectly-drained	125 - 500	25 - 150	>20 *<50*	15 – 30 *67 - 33*	Boulders P, M Groundwater L, W - M Basal contact L, W - M	400 - 600	280 - 380
Unit 3 */** Glacio-lacustrine	Clay and silt; deformed; stiff to hard; poorly-drained	<125	25 – 100	>20 *<50*	15 – 30 *67 - 33*	Groundwater L, W - M Basal contact L, M - S	1400 – 2300	300 - 500
Unit 2 */** Colluvial	Clay, poorly-drained, stiff to hard; and blocks, gravel, sand, clast-supported diamicton; imperfectly-drained	<500	150 – 500	<20 *>50*	15 – 30 *67 - 33*	Basal contact L, M - S	600 - 3500	380 - 500
Unit 1 **/*** Bedrock *May contain*	Andesite, rhyolite and pyroclastic beds; weathered,	>500	1,000 - >3,000	<5 *>200*	<15 *>67*	No internal reflectors	3500 - 4000 (weathered)	500 - 700

ground-water	fractured; well-drained	>4000 (pristine)

928

929

930

931

932

933 **Figures**

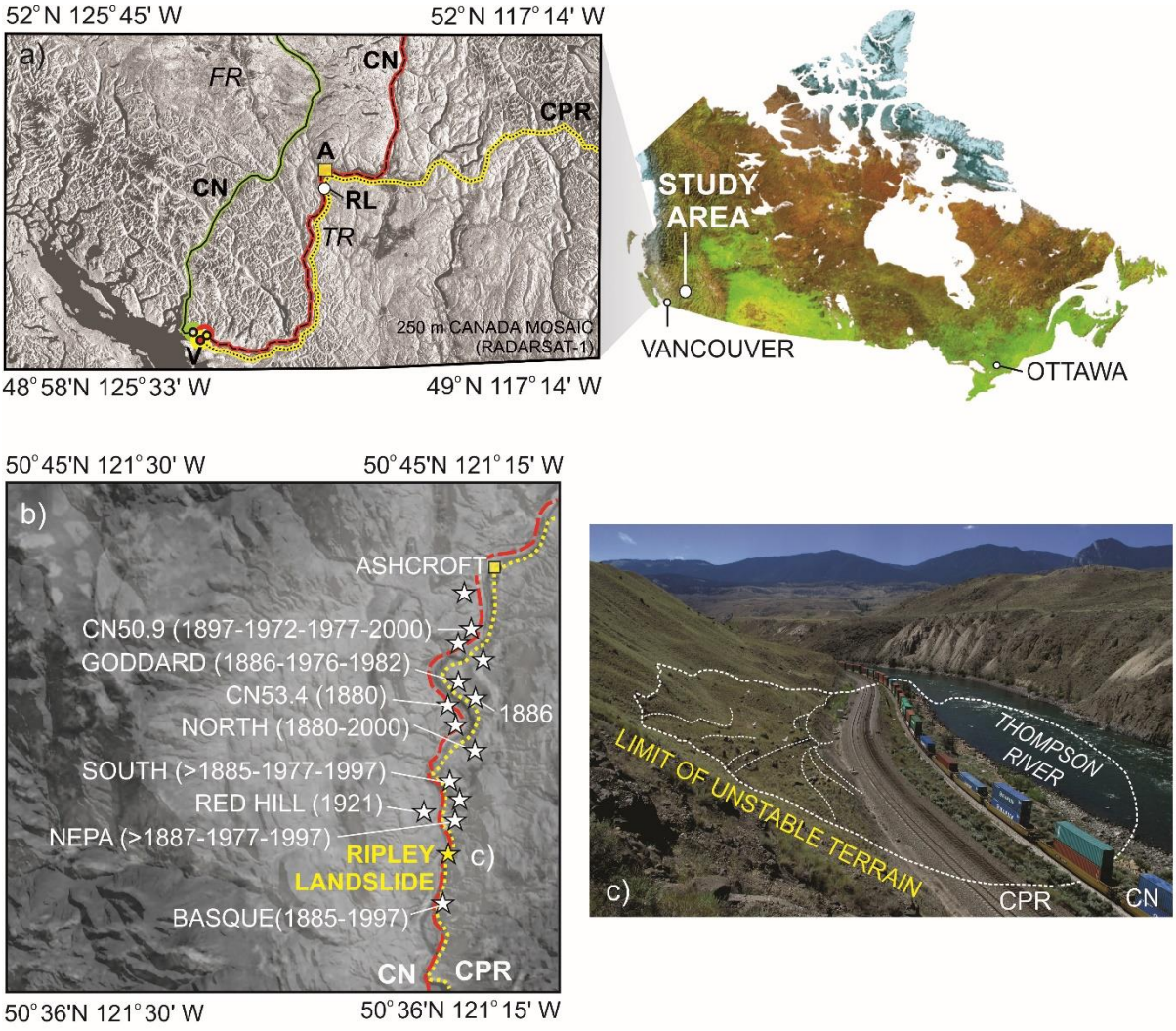

934
935
936 **Fig. 1** The study area. a) Rail transportation corridors in southwestern British Columbia with location of the
937 Thompson River valley area of interest: **A** – Ashcroft; **K** – Kamloops; **L** – Lytton; **S** – Spences Bridge; **V** –
938 Vancouver; **FR** – Fraser River; **TR** - Thompson River. b) Landslides of the Thompson River valley, with location
939 of Ashcroft, the railway transportation corridor and Ripley Landslide test site. c) Overview of the test site
940 highlighting the approximate limit of unstable terrain and submerged slide toe.
941

Fig. 2 Hydrogeological units of Ripley Landslide. a) Unit 1a- andesite: fine-grained crystalline igneous rock with dominant fractures 040º/076º/E (278 m elevation), 074º/50º/NNW, 136º/78º/W, 178º/28º/E. b) Unit 1b - rhyolite and pyroclastic volcanic rock: strike/dip/dip-direction 104º/18º/E (350 m elevation). c) Unit 2 – colluvial sediments: interbedded clast-supported diamicton, sand and gravel overlying fractured bedrock (unit 1), ca. 276 m elevation. d) Unit 3 - glaciolacustrine sediments: rhythmically interbedded clay, silt and sand with rare dropstones; sub-till (unit 4) soft-sediment indicates glacial deformation, ca. 278 m elevation. e) Unit 4 – lodgement till: massive, matrix-supported diamicton overlain by a veneer of hillslope colluvium (unit 8) exposed in headscarp; at 280 m elevation. f) Unit 5 - glaciolacustrine sediments: interbedded silt and clay overlying till (unit 4), silt-rich beds appear lighter; bedding-parallel fissility and vertical slope relaxation fractures formed in exposed in railway embankment. g) Unit 6 - glaciofluvial sediments: cobble gravel and sand; moderately steep slope (25 º - 32º) is

gullied and drains a 340 m - 350 m elevation terrace abutting against bedrock (unit 1b). h) Unit 7 - alluvial fan sediments: silt, sand and gravel deposited on outwash and till as terraced fans with slopes up to 12°; indicate falling base-levels in the Thompson River valley during early Holocene. i) Unit 8 - colluvial sediments: erratic boulders, glaciofluvial cobbles and sand remobilized by debris fall, soil creep and surface runoff on slopes ranging from 25° slope above the headscarp to 12° across the main slide body; on steeper portions of the slope (up to 32°), talus blocks are derived from frost shattered rhyolite and volcaniclastic rock. j) Unit 9 - alluvial floodplain sediments: boulders, cobbles and sand, sparse vegetation growth dominated by horsetails indicating zone of seepage across the landslide toe. k) Unit 10 - anthropogenic features: boulder-rich track ballast overlying alluvial floodplain on the landslide toe; CN (top left) and CPR tracks (centre); l) Unit 10 - lock-block retaining wall separating CPR (above left) and CN tracks (right).

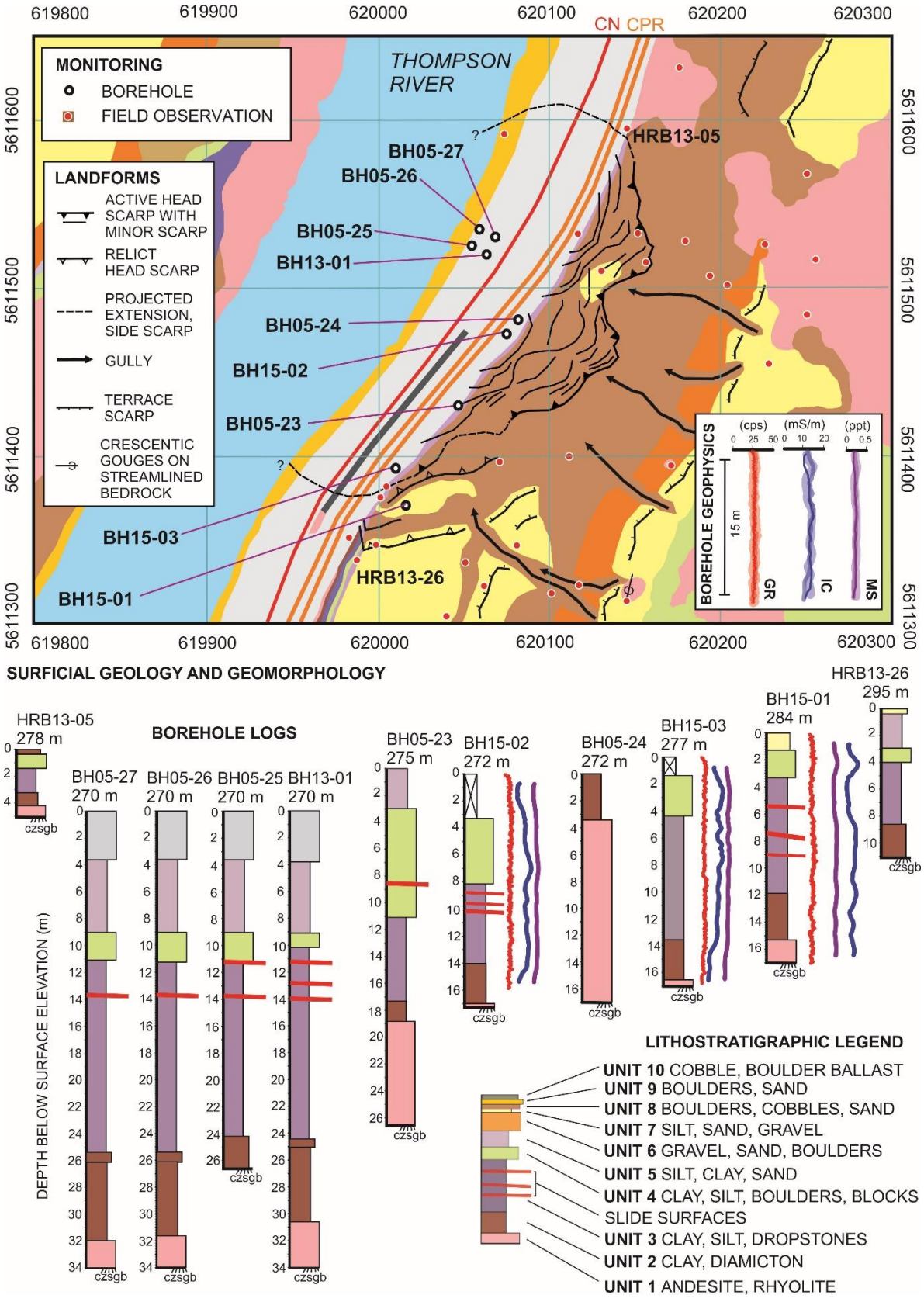

Fig. 3 Surficial hydrogeological units and landforms of Ripley Landslide and adjacent terrain, showing location of boreholes and field observations; lock-block retaining wall – grey line. Borehole geophysical logging and data processing by Frontier Geosciences Inc.

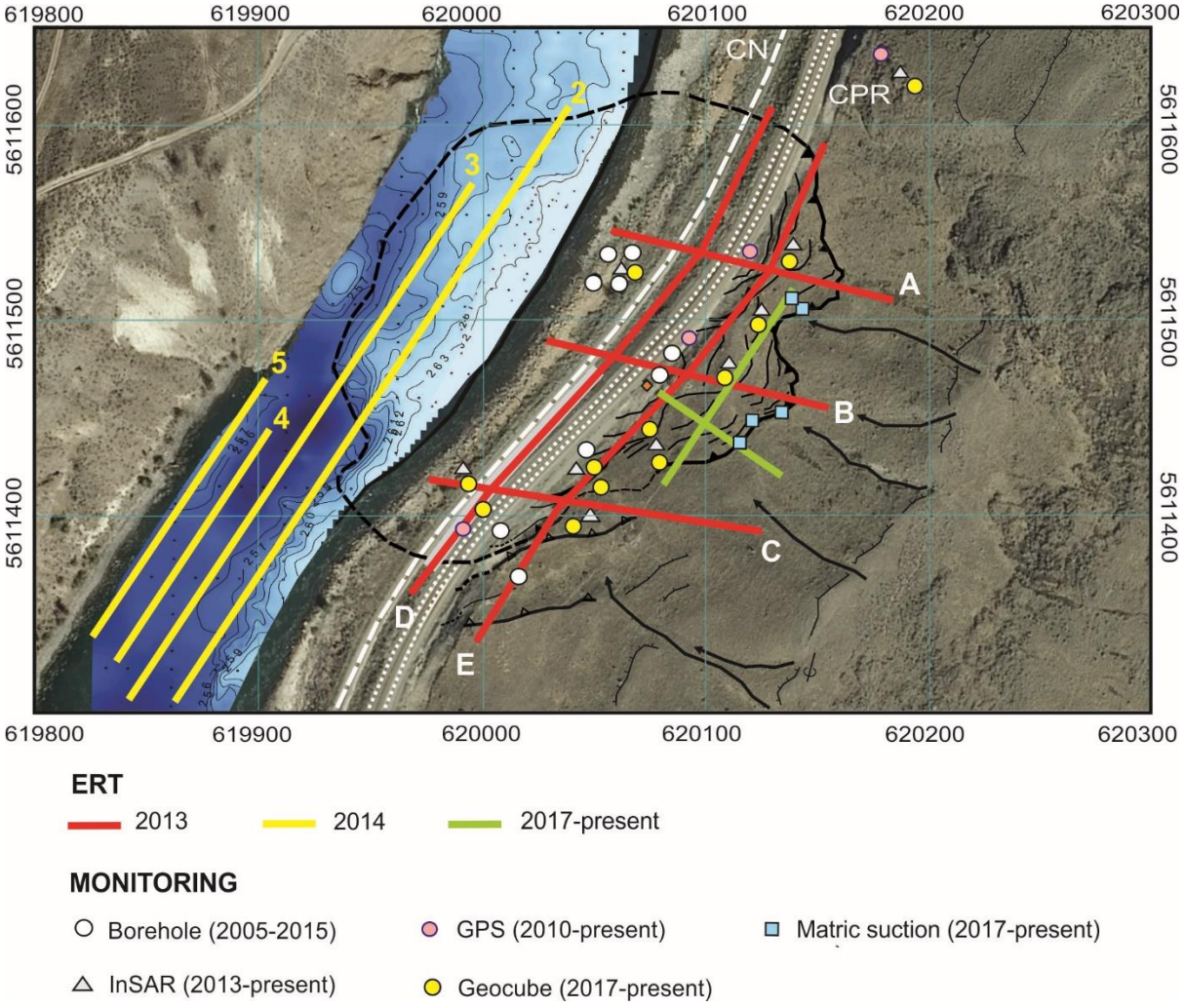

Fig. 4 Geophysical transects for November 2013 (red lines), November 2014 (yellow lines), and PRIME installation, beginning in November 2017 (green lines); other monitoring components shown include positions of logged boreholes (2005-2015), InSAR corner reflectors (2013 - present) and permanent GNSS stations (2010 – present).

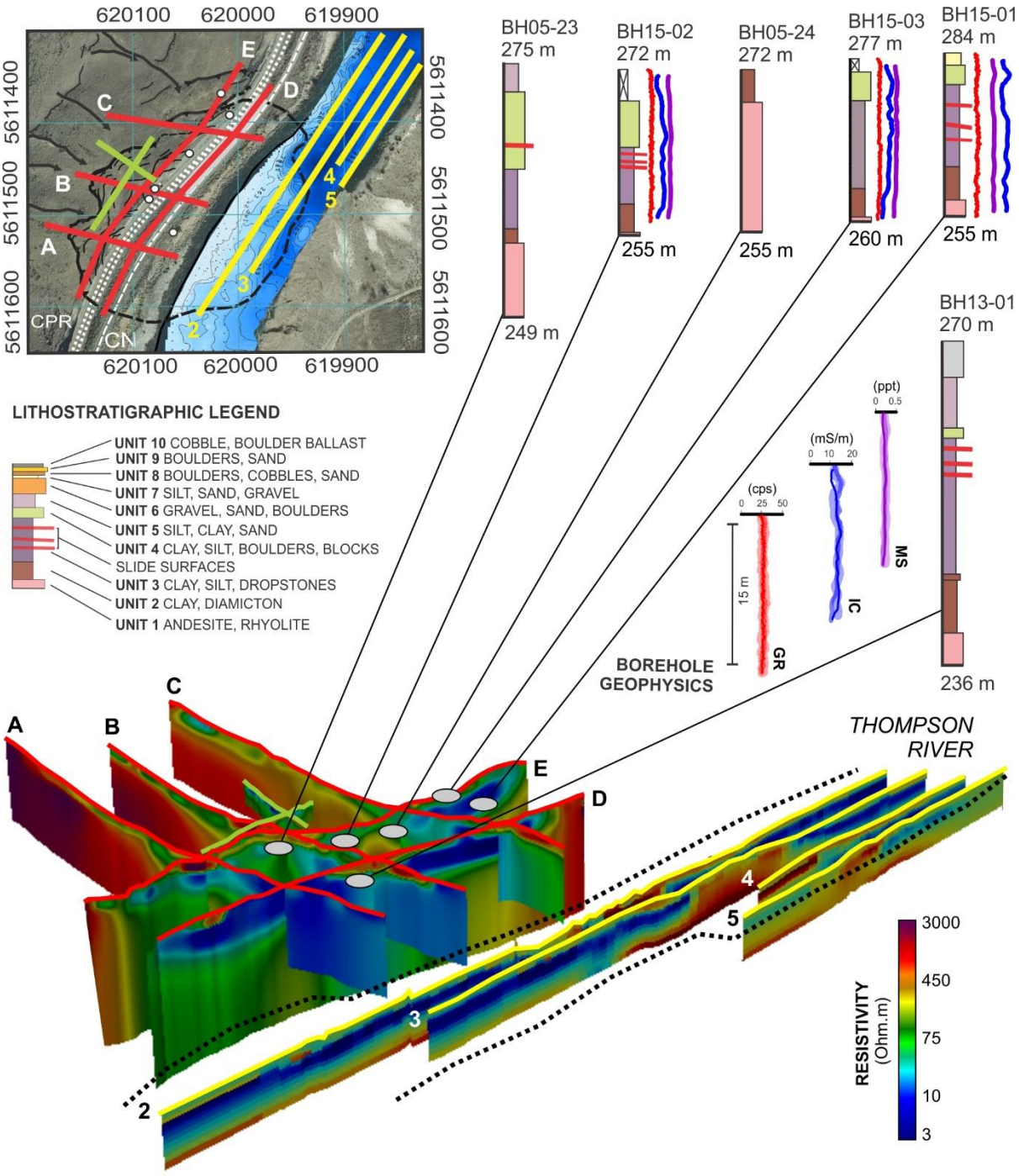

Fig. 5 Terrestrial ERT pseudosections (red transect lines A, B, C), waterborne ERT pseudosections (yellow transect lines 2, 3, 4, 5) and PRIME installation (green transect lines). Location of boreholes shown in relation to transect lines. Gamma radiation measured in counts per second (cps), induced conductivity measured in milliSiemens/m (mS/m) and magnetic susceptibility in parts per thousand (ppt)**.** Also shown, location of elevated terrain conductivity readings located on submerged slide toe. Landslide extent (approximate) shown as dashed black lines on inset map.

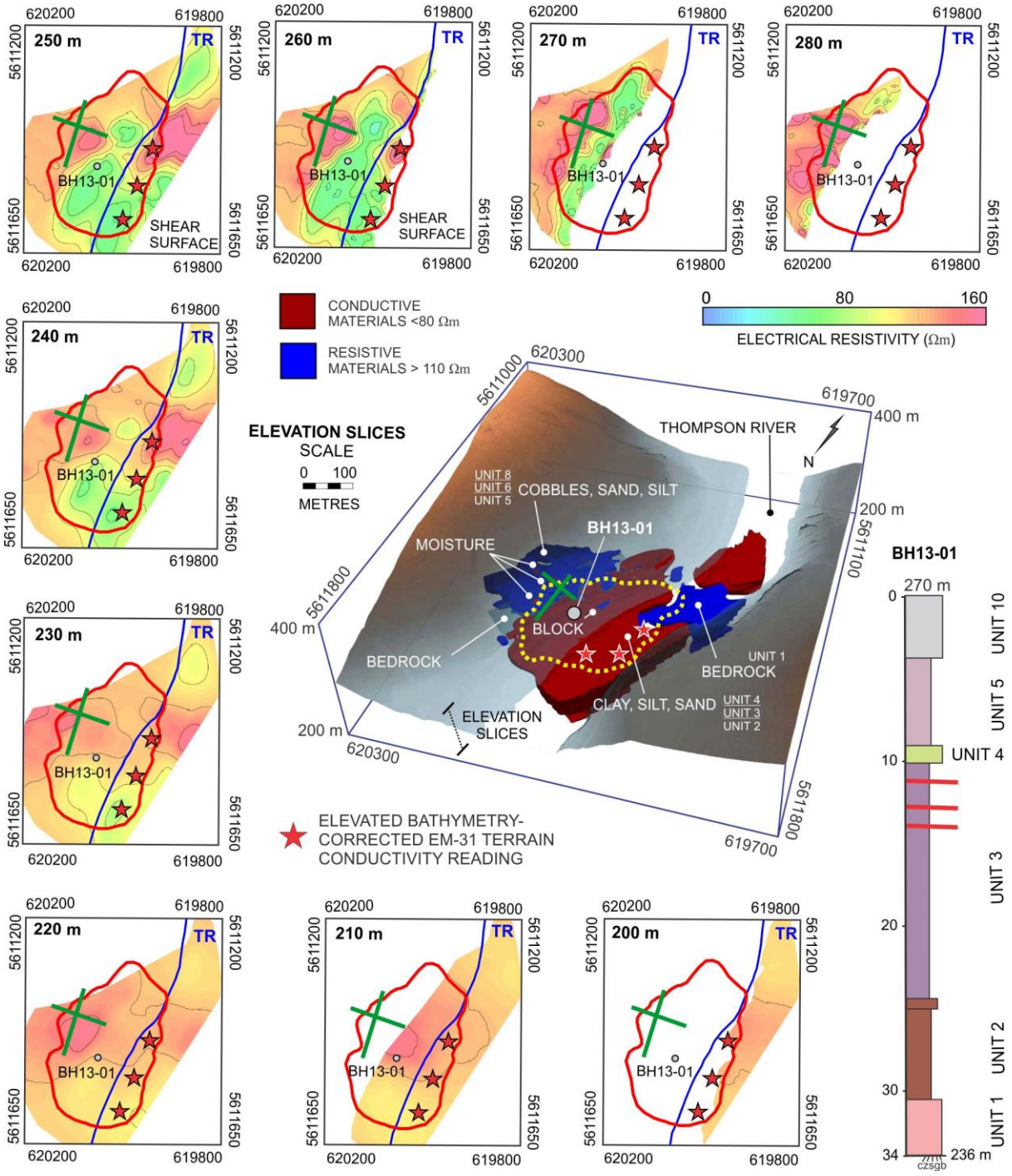

979

980 **Fig. 6** Electrical resistivity tomographic depth slices of Ripley Landslide. Location of BH13-01 shown; graphic
981 log captures changes in hydrogeological units at depth near the centre of the slide body. Solid blue line – east bank
982 of Thompson River (**TR**). Solid green line - PRIME array. Red stars indicate elevated bathymetry-corrected EM
983 terrain conductivity interpreted as artesian groundwater discharge zones exposed by river erosion. Data processing
984 by Frontier Geosciences Inc.

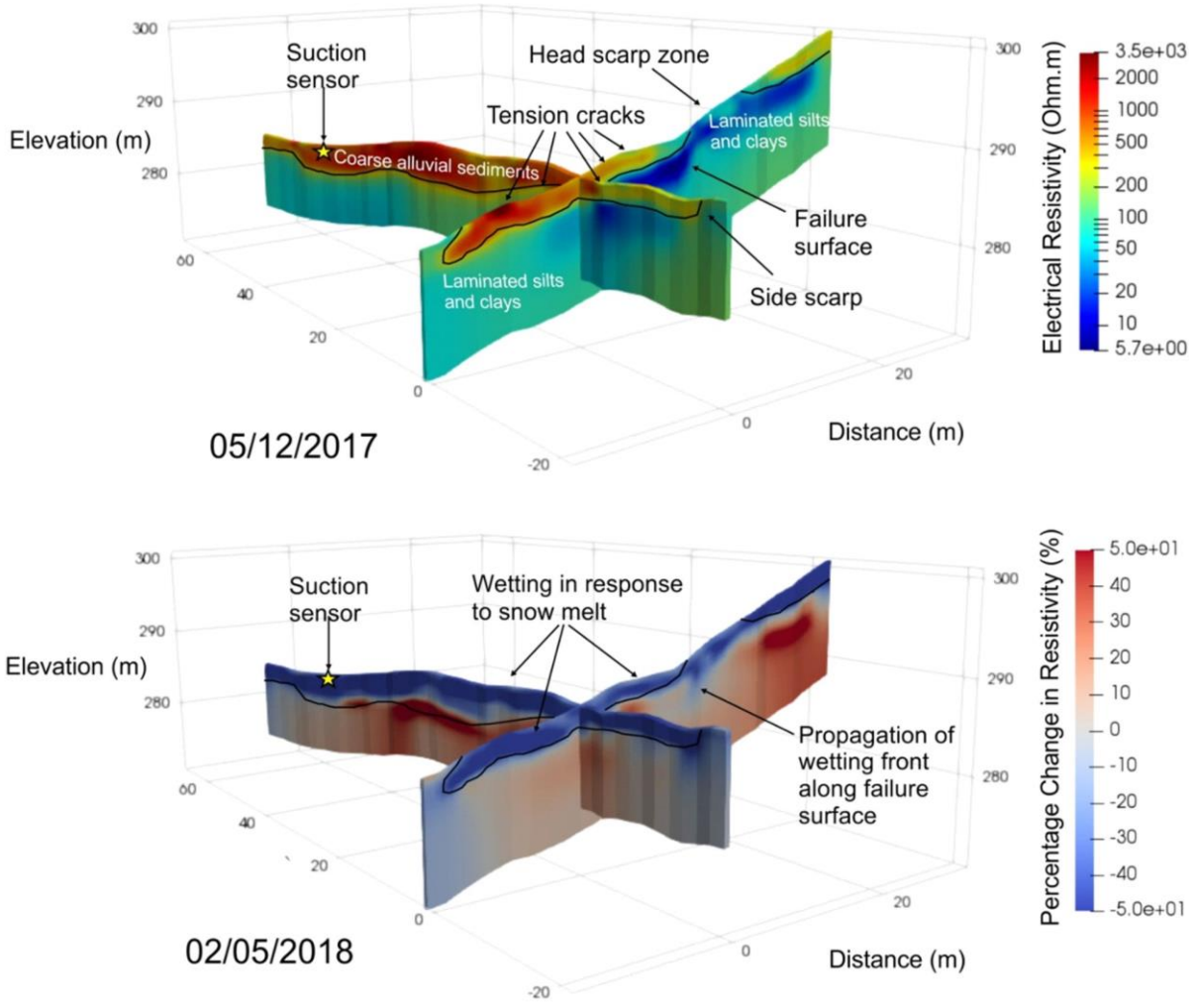

985

986 **Fig. 7** Electrical resistivity tomography images generated from the PRIME data collected on the Ripley landslide.
987 The baseline image (December 05, 2017) highlights the lithological units present on site and shows key
988 geomorphological features including failure surfaces and tension cracks. The image from May 02, 2018 shows the
989 percentage change in resistivity from the baseline image, highlighting changes which took place following the
990 onset of snowmelt on the site. Suction sensor locations are marked by the yellow stars. The suction sensors (yellow
991 star) are located at 0.3 m, 0.6 m, 0.9 m, 1.2 m and 2 m below the surface.

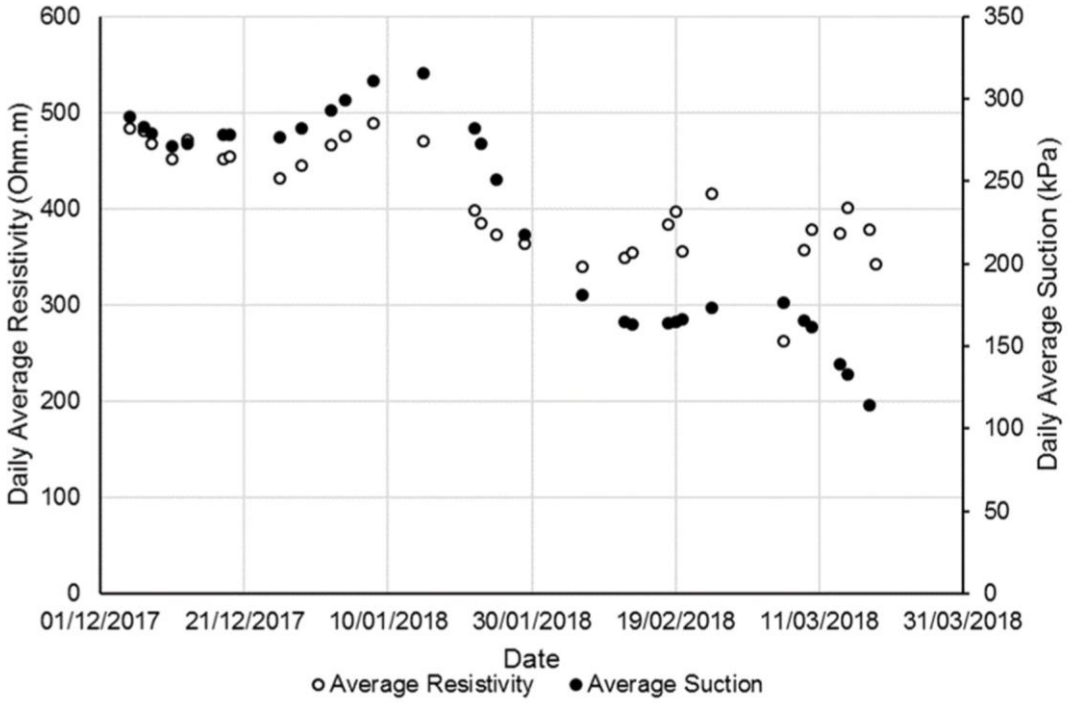

992

993 **Fig. 8** Relationship between resistivity and suction for the Ripley landslide head scarp. The average daily
994 resistivity is the average resistivity of cells of the PRIME model (**Fig. 7**) proximal to the suction sensors (within
995 1 m distance). The suction sensors are located at 2, 3, 4, and 6.5 ft depth from the surface, and their location
996 relative to the PRIME ERT lines is shown in **Fig. 7**.